Redshift leverage for the search of GRB neutrinos affected by quantum properties of spacetime

Journal of Cosmology and Astroparticle Physics
An IOP and SISSA journal

Received: May 23, 2025
Revised: September 23, 2025
Accepted: December 2, 2025
Published: February 11, 2026

Redshift leverage for the search of GRB neutrinos affected by quantum properties of spacetime

Giovanni Amelino-Camelia,[a,b] **Giacomo D'Amico**,[c,d] **Vittorio D'Esposito**,[a,b] **Giuseppe Fabiano**,[e,f,g] **Domenico Frattulillo**,[b] **Giulia Gubitosi**,[a,b,*] **Dafne Guetta**,[h] **Alessandro Moia**[a] **and Giacomo Rosati**[i,j,k]

[a] *Dipartimento di Fisica Ettore Pancini, Università di Napoli "Federico II", Complesso Univ. Monte S. Angelo, I-80126 Napoli, Italy*
[b] *Istituto Nazionale di Fisica Nucleare, Sezione di Napoli, Complesso Univ. Monte S. Angelo, I-80126 Napoli, Italy*
[c] *Institut de Física d'Altes Energies (IFAE), The Barcelona Institute of Science and Technology (BIST), E-08193 Bellaterra (Barcelona), Spain*
[d] *Department for Physics and Technology, University of Bergen, NO-5020 Bergen, Norway*
[e] *Physics Division, Lawrence Berkeley National Laboratory, Berkeley, CA 94720, U.S.A.*
[f] *Department of Physics, University of California, Berkeley, CA 94720, U.S.A.*
[g] *Centro Ricerche Enrico Fermi, I-00184 Rome, Italy*
[h] *Capodimonte Observatory, INAF-Naples, Salita Moiariello 16, 80131 Napoli, Italy*
[i] *Institute for Theoretical Physics, University of Wrocław, Pl. Maksa Borna 9, Pl–50-204 Wrocław, Poland*
[j] *Dipartimento di Matematica, Università di Cagliari, via Ospedale 72, 09124 Cagliari, Italy*
[k] *Istituto Nazionale di Fisica Nucleare, Sezione di Cagliari, Cittadella Universitaria, 09042 Monserrato, Italy*

E-mail: giovanni.amelinocamelia@unina.it, gdamico@ifae.es, vittorio.desposito@roma2.infn.it, gfabiano@lbl.gov, domenico.frattulillo@unina.it, giulia.gubitosi@unina.it, dafneguetta@gmail.com, alessandro.moia@unina.it, giacomo.rosati@unica.it

Abstract: Some previous studies based on IceCube neutrinos had found intriguing preliminary evidence that some of them might be GRB neutrinos with travel times affected by quantum properties of spacetime delaying them proportionally to their energy, an effect often

*Corresponding author.

https://doi.org/10.1088/1475-7516/2026/02/035

JCAP02(2026)035

labeled as "quantum-spacetime-induced in-vacuo dispersion". Those previous studies looked for candidate GRB neutrinos in a fixed (neutrino-energy-independent) time window after the GRB onset and relied rather crucially on crude estimates of the redshift of GRBs whose redshift has not been measured. We here introduce a complementary approach to the search of quantum-spacetime-affected GRB neutrinos which restricts the analysis to GRBs of sharply known redshift, and, in a way that we argue is synergistic with having sharp information on redshift, adopts a neutrino-energy-dependent time window. We find that knowing the redshift of the GRBs strengthens the analysis enough to compensate for the fact that of course the restriction to GRBs of known redshift reduces the number of candidate GRB neutrinos. And rather remarkably our estimate of the magnitude of the in-vacuo-dispersion effects is fully consistent with what had been found using the previous approach. Our findings are still inconclusive, since their significance is quantified by a p-value of little less than 0.01, but provide motivation for monitoring the accrual of neutrino observations by IceCube and KM3NeT as well as for further refinements of the strategy of analysis here proposed.

Keywords: quantum gravity phenomenology, ultra high energy photons and neutrinos

ArXiv ePrint: 2501.13840

JCAP02(2026)035

Contents

1 Introduction and new selection criteria

The current generation of neutrino telescopes was devised to mark the start of neutrino astrophysics, and indeed IceCube firmly established the observation of cosmological neutrinos [1], but so far not much astrophysics has been done with neutrinos: there is only evidence of a neutrino signal from the active galaxy NGC 1068 [2] and from the flaring blazar TXS 0506+056 (see, e.g., refs. [3, 4]). With respect to pre-IceCube expectations what is clearly missing are observations of neutrinos from GRBs (gamma-ray bursts). The prediction of a neutrino emission associated with GRBs is generic within the most widely accepted astrophysical models [5] and pre-IceCube studies estimated about a handful of GRB-neutrino observations per year of operation [6–9]; yet, as IceCube nears 15 years of operation, still not a single GRB neutrino has been reported. The simplest (and most likely) explanation of this lack of observations of GRB neutrinos is that our GRB models must be revised in such a way to produce a much lower neutrino flux, but it is intriguing that in principle one could also invoke some plausible quantum properties of spacetime which had already been investigated for independent reasons in the quantum-gravity literature: IceCube searches might have failed to find GRB neutrinos because they assume that a GRB neutrino should be detected in very close temporal coincidence with the associated gamma rays, but a sizable mismatch between the neutrino detection time and the time of detection of the electromagnetic GRB signal would be expected in presence of "in-vacuo dispersion", a much-studied effect such

JCAP02(2026)035

that quantum properties of spacetime slow down[1] particles proportionally to their energies (see, e.g., refs. [10–19] and references therein).

We here focus exclusively on the most studied scenario for in-vacuo dispersion which for our purposes is conveniently characterized in terms of the following relationship [20–24]:

$$\Delta t = \eta D(z) \frac{E}{M_P} \,, \tag{1.1}$$

where Δt is the contribution to the travel time of the neutrino due to quantum-gravity-induced in-vacuo dispersion, E is the neutrino energy, M_P denotes the Planck scale ($\sim 10^{16}$ TeV), and $D(z)$ is a function of the redshift z of the source,

$$D(z) = \int_0^z d\zeta \frac{(1+\zeta)}{H_0 \sqrt{\Omega_\Lambda + (1+\zeta)^3 \Omega_m}}$$

(Ω_Λ, H_0 and Ω_m denote, as usual, respectively the cosmological constant, the Hubble parameter and the matter fraction, for which we take the values given in ref. [25]).

We restrict to the scenario with purely systematic effects, in which η is simply a parameter to be determined experimentally. When a larger collection of astrophysical neutrinos becomes available (and therefore analyses such as ours can attempt multi-parameter investigations), it will be possible to consider the more general case of a mixture of systematic and fuzzy effects [18, 19, 26], in which η is described as a random variable (taking different values for different neutrinos) with mean η_0 and dispersion $\delta\eta$. We also postpone the extension of our phenomenological model to allow for the possibility that there might be intrinsic at-the-source effects causing a sizable offset between the typical neutrino emission time and the GRB onset. A first step for modeling the impact of such intrinsic effects on in-vacuo dispersion analyses would be to add to eq. (1.1) an extra term of the form $\bar{\tau}(1+z)$, where $\bar{\tau}$ is the average neutrino emission time offset with respect to the GRB onset and the factor $(1+z)$ accounts for ordinary time dilation, but investigations of such a refined model need more astrophysical neutrinos than presently available.

The effects of eq. (1.1) are totally unnoticeable on terrestrial scales, but for the observation of distant astrophysical sources the factor $D(z)$ can be large enough to compensate for the Planck-scale suppression [10–19].

Indeed, in-vacuo dispersion for photons has been investigated very intensely over the last 15 years (see, e.g., refs. [18, 19] and references therein), with some studies even reaching sensitivity of the order of the Planck scale (see, e.g., ref. [27]). It is difficult to say exactly which values of η have been excluded for photons, since the magnitude of in-vacuo-dispersion effects could be comparable to known (but poorly understood) intrinsic spectral lags and a delayed emission of the relevant photons cannot be ruled out (some of the most energetic photons from a GRB could be emitted within the long afterglow phase). Still, a balanced perspective is that, for photons, we are close to Planck-scale sensitivity [18, 19].

The investigation of in-vacuo dispersion for neutrinos has been lagging far behind: the current bound on in-vacuo dispersion for neutrinos is still based on the historic observation

[1] While the theoretical prejudice of most quantum-spacetime researchers favors effects that slow down particles, there is no conclusive theoretical argument ruling out that quantum-spacetime effects might instead speed up particles. We offer some data-based observations relevant for this issue in parts of section 5.

JCAP02(2026)035

of neutrinos from the SN1987a supernova, and only amounts to $\eta \lesssim 10^9$ [28]. This is very unsatisfactory, especially in light of the fact that the quantum-spacetime literature provides motivation for studying in-vacuo dispersion for photons and neutrinos separately. In particular, quantum-spacetime models based on Planck-scale discretization predict in-vacuo dispersion for neutrinos but not for photons [14, 29], and this is consistent with results from models based on causal sets [30]. Moreover, within a popular effective-theory approach to quantum-spacetime properties one describes in-vacuo dispersion for neutrinos in a way that is completely independent from that applicable to photons [16]. Given the typical energies of the astrophysical neutrinos observed by current telescopes, even just a single observation of a GRB neutrino would allow us to constrain in-vacuo dispersion for neutrinos rather tightly. However, as mentioned at the beginning, no such observation has been reported yet by studies assuming no in-vacuo dispersion.

As observed in refs. [20–24, 31, 32] the search of GRB neutrinos affected by in-vacuo dispersion must necessarily rely on a statistical approach: we could never be sure that a certain neutrino is a GRB neutrino, but we might at some point observe enough GRB-neutrino candidates (neutrinos that could come from a GRB, assuming in-vacuo dispersion) to be sure that at least some of them are actually GRB neutrinos affected by in-vacuo dispersion. This is due to the size of the time window that one must adopt in order to investigate the hypothesis of in-vacuo dispersion. Standard searches of GRB neutrinos (assuming $\eta = 0$, no in-vacuo dispersion) can assume that the neutrino and the electromagnetic signal from the GRB travel essentially at the same speed, and therefore their GRB-neutrino candidates are looked for within a tiny time window, rendering background issues insignificant. For $\eta \neq 0$, also taking into account that the neutrino energy will have some uncertainty (and however one will inevitably always end up testing an hypothesis of η taking values in a certain range), the difference in observation time between the neutrino and the electromagnetic signal would be sizably uncertain, and the time window for searches of GRB-neutrino candidates would have to be correspondingly large, resulting in background issues such that one could not be sure that a specific GRB-neutrino association is correct.

Evidently the effectiveness of such a statistical approach depends rather crucially on the criteria used for the selection of candidate GRB neutrinos. And our main objective here is to test a novel proposal for these criteria. Testing alternative strategies of analysis on presently-available IceCube data is also important because it can set the stage for a later, more mature, phase of the research program, eventually using also data from KM3Net [33] and IceCube-Gen2 [34].

Previous searches [20–24, 31, 32] of GRB neutrinos affected by in-vacuo dispersion looked for neutrinos within a time window of fixed size (neutrino-energy-independent) after the GRB onset, and put on the same footing both GRBs whose redshift has not been measured (then having to estimate that redshift crudely, since the conjectured effect is redshift dependent) and GRBs of known redshift. Including GRBs whose redshift has not been measured has the advantage of a larger number of candidate GRB neutrinos, but of course renders the analysis vulnerable to the assumptions made to roughly estimate the redshifts. Moreover, the fixed-size time window, while easily handled computationally, imposes a restriction of the analysis to a corresponding limited range of neutrino energies: since the sought effect grows

JCAP02(2026)035

linearly with energy, a time window adapted to energies of, say, 100 TeV will inevitably be too small for neutrinos with energy much greater than 100 TeV, and in an appropriate sense it would also be too large a time window for neutrinos of energy smaller than 100 TeV (when the time window is much wider than the one really needed by the sought effect, the analysis ends up being dominated by the background). In spite of these limitations, ref. [32], the latest such study (of which some of us were authors), provided the estimate $\eta = 21.7 \pm 4.5$ with a p-value[2] $P_{[34]} = 0.007$.

We here take the results of ref. [32] as a starting point for testing a novel strategy of analysis. Rather than adopting a fixed-size time window and correspondingly restricting the neutrino-energy range, we consider all the neutrinos in the sample, regardless of the energy, but restrict the GRB catalogue to GRBs of known redshift. Any GRB and neutrino times of arrival are then regarded as compatible if they satisfy eq. (1.1) for some $\eta \in [12.7, 30.7]$ (the two-standard-deviation interval obtained from the estimate $\eta = 21.7 \pm 4.5$ found in ref. [32]) within two standard uncertainties in the neutrino energy. As here shown in section 4, the fact that, by relying exclusively on GRBs of known redshift, we find fewer GRB-neutrino candidates is more than compensated, for what concerns the overall statistical significance, by the sharper setup of the analysis which is available when the redshift of the GRBs is known.

Also for what concerns the assessment of the directional compatibility between a neutrino and a GRB the criteria here adopted differ from those of previous analogous studies. This change, however, does not reflect a strategic choice: it is rather due to a qualitative upgrade in the neutrino directional information provided by IceCube. Previous IceCube data releases provided neutrino directional information adopting a rather crude approximation, resulting in gaussian uncertainties. In that case, since the angular positions of the overwhelming majority of GRBs (including all known-redshift GRBs) are also affected by gaussian uncertainties, the directional compatibility between a neutrino and a GRB can be naturally assessed computing the angular separation $\Delta\theta$ between the respective mean directions and comparing it with the combined angular uncertainty $\sigma = \sqrt{\sigma_{\rm GRB}^2 + \sigma_\nu^2}$. This was done, e.g., in ref. [32], where a neutrino and a GRB were regarded as directionally compatible if $\Delta\theta \leq 3\sigma$. The latest IceCube HESE data release (see section 2) characterizes the uncertainty in the direction of each neutrino in terms of an 8-parameter Fisher-Bingham (FB8) distribution $P_\nu(\Omega)$ on the sphere [35]. These FB8 distributions are quite complex angular distributions, as they are in most cases multimodal and very asymmetric. As a result, the very notions of angular separation $\Delta\theta$ and combined angular uncertainty σ lose their well-defined gaussian meaning, and a different, more general criterion is needed to assess the directional compatibility between a neutrino and a GRB. Here we follow other studies that handled similarly complex directional uncertainties (see, e.g., ref. [36]) and compute for each GRB-neutrino pair the value of the statistic $\mathcal{S} = \int P_\nu(\Omega) P_{\rm GRB}(\Omega) d\Omega$, where $P_\nu(\Omega)$ is the FB8 uncertainty on the direction of the neutrino (taken from the HESE data release) and $P_{\rm GRB}(\Omega)$ is the gaussian uncertainty on the position of the GRB (reconstructed from the angular information collected in our GRB

[2] As will be clearer for our readers when, later in this manuscript, we derive an analogous p-value for our novel selection criteria, this p-value, which in ref. [32] was called false alarm probability, is the probability to find at least as many (and as good) GRB-neutrino candidates as were actually found in the data under the null hypothesis of no in-vacuo dispersion ($\eta = 0$), whereas $\eta = 21.7 \pm 4.5$ is an estimate of η obtained from the actually found GRB-neutrino candidates.

JCAP02(2026)035

catalogue; see section 2 and appendix A). This $\mathcal{S}$ can be computed for angular distributions of arbitrary shape and is a good measure [36] of angular compatibility (in particular, its value increases as the highest density regions of the two distributions grow closer on average). One can then regard the directions of a GRB-neutrino pair as compatible if the corresponding $\mathcal{S}$ satisfies $\mathcal{S} \geq \mathcal{S}_{\rm cut}$ for some fixed reference value $\mathcal{S}_{\rm cut}$. In setting up this exploratory study we adopted $\mathcal{S}_{\rm cut} = 1/4\pi$, which is the value taken by $\mathcal{S}$ whenever one of the distributions is the uniform distribution on the sphere. This choice is intuitively natural, as it would be difficult to claim any degree of directional compatibility if two uniform, uninformative distributions would be given a better score. We also checked on previous releases of IceCube data (those affected by the rough, approximate gaussian uncertainties mentioned above) that on those data the effect of the new requirement $\mathcal{S}_{\rm cut} = 1/4\pi$ is very similar to the effect of the criterion $\Delta\theta \leq 3\sigma$ adopted in previous studies. More significantly, the results reported in the following sections show that the choice $\mathcal{S}_{\rm cut} = 1/4\pi$ is indeed a good starting point for this research program (mainly because the noise level it introduces, as observed in section 3, is tolerable). However, as this research program gradually matures, it will be important to investigate what is the optimal choice of $S_{\rm cut}$, since the discovery potential of statistical approaches such as ours can depend strongly on these choices: higher(/lower) values of $S_{\rm cut}$ will decrease(/increase) the chances of picking up background but also increase(/decrease) the chances of losing signal, and an optimization would of course be advantageous. Statistical optimizations of this kind are themselves challenging research projects, and we postpone a full effort to future studies; however, after performing our main analysis (here reported in section 4), we explored the dependence of our results on the choice of $\mathcal{S}_{\rm cut}$, finding preliminary evidence that $\mathcal{S}_{\rm cut} = 1/4\pi$ might not be too far from optimal (see section 5).

2 IceCube neutrinos and GRBs of known redshift

Our analysis relies on the latest HESE data release by IceCube (7 September 2023), available at [37]. We chose to work with the HESE sample because it is the IceCube sample least contaminated by atmospheric neutrinos, especially above 50–60 TeV [38]. As done in previous analogous studies [20–24, 32], we restrict to shower (or cascade) events, since track events have very poor energy estimates (and of course the quality of the energy information is crucial for in-vacuo-dispersion studies) [39, 40]. An additional advantage of working with shower events is that they are even more robust against atmospheric contamination (for the shower morphology, the atmospheric neutrino flux above 1 TeV is suppressed by about an order of magnitude with respect to the track morphology [41]).

A sizable part of the effort we devoted to this study was aimed at compiling a reliable catalogue of GRBs with actually measured (and not just estimated or loosely constrained) redshifts. In fact, we found that all already available GRB catalogues either imposed further constraints on the GRB properties (narrower observation window, restriction to specific GRB observatories, GRB type, etc.) or were not sufficiently accurate (misreporting or omitting direction or redshift data, not taking into account the latest relevant GCNs, etc.). The resulting list is reported here in appendix A. In about 90% of cases it agrees with an analogous general-purpose catalogue, not restricted to known-redshift GRBs, maintained by the IceCube collaboration [42]. The previous study [32] relied on this resource, but, after checking one-

JCAP02(2026)035

by-one each of its known-redshift entries, we noticed that some of the information relevant for our analysis was inaccurately reported, probably due to the automated population of the database. In most cases this was quickly corrected according to the web catalogue [43] maintained by Jochen Greiner at the MPE, which we found to be the most accurate and comprehensive among publicly available lists. Checking by hand all the relevant GCNs and consulting additional catalogues of known-redshift GRBs, we were then able to correct the few errors left and also identify a few known-redshift GRBs whose redshift is not reported in Greiner's table (see appendix A for details).

In the end, all these efforts did not actually pay off in terms of a significant improvement of our analysis: as regards the four GRBs of known redshift playing a crucial role in our main analysis (see section 4), our corrected and augmented catalogue agrees with both [42] and [43]. Still, we hope that the effort we put in preparing appendix A will be of service to the community. In particular, our appendix A should represent a tangible improvement over both [42] and [43] for researchers exploring alternative search strategies for GRB neutrinos affected by in-vacuo dispersion.

3 Simulated data for the statistical-significance analysis and background estimate

As stressed above, the in-vacuo-dispersion significance of our findings can only be investigated using a statistical approach based on the p-value, i.e. estimating numerically the probability that one could find GRB-neutrino candidates in such good agreement with the in-vacuo-dispersion hypothesis just by accident, as an outlier of the type of findings one would expect within the null hypothesis $\eta = 0$ of no in-vacuo dispersion.

As done in the previous neutrino studies[3] of refs. [21–23], we do this by producing simulated data through transformations of the real data which reliably preserve their morphology while washing away any possible correlations of the type predicted by eq. (1.1) between the time of arrival, the neutrino energy, and $D(z)$.

Our simulated data are obtained from the real data performing the following independent manipulations:

- we act on the neutrino observation times with a random permutation (i.e., we sort the observation times in a random order while keeping the neutrino list fixed) followed by a random periodic time translation (the periodicity makes it sure that they stay within the actual IceCube observation window);
- we act on the neutrino directions with a rotation of a random angle around the Earth's axis;
- we act on the GRB directions with a random permutation (see above) followed by a rotation of a random angle around the Galactic axis.

  A combination of these manipulations is arguably the most general transformation of the true data not affecting their morphology in any relevant respect. In fact:

[3] The interested reader can find applications of this method of statistical analysis to studies not involving neutrinos, e.g., in refs. [36, 44–48].

JCAP02(2026)035

- the neutrino observation times are statistically compatible with their being uniformly distributed within the IceCube observation window, and there are no a-priori reason for expecting a change in the HESE neutrino rate in this period;

- the efficiency of the IceCube detector, whose axis is closely aligned to the Earth's axis, is virtually independent of the right ascension, but not of the declination, of incoming neutrinos, as clearly evidenced in the neutrino angular data; we choose not to reshuffle the neutrino directions so as not to spoil their evident correlation with the neutrino energies (the higher the neutrino energy, the more accurate its reconstructed direction);

- the directions of known-redshift GRBs are independent of galactic longitude, but are correlated to some extent with galactic latitude, as the dust lying around the galactic plane makes it much more difficult to determine the redshift of a GRB in that region; also, we do not act on the GRB observation times because we find that the detection rate of known-redshift GRBs is declining with time, probably another selection effect due to older events having been more likely followed by the long-term, host-galaxy observations which are often needed to determine the redshift of a GRB.

As a first application of our simulated data we can estimate the overall background that is expected with the criteria adopted by our strategy of analysis. For this purpose, we generated 10^5 instances of simulated data[4] and we used them to estimate the expected number of HESE shower neutrinos that in the absence of in-vacuo dispersion could accidentally be associated with a GRB of known redshift according to the time-energy and direction compatibility conditions specified above (with $\eta \in [12.7, 30.7]$ and $\mathcal{S}_{\rm cut} = 1/4\pi$). We find that, on average, our criteria should pick up 1.02 such accidental GRB-neutrino associations.

4 Main analysis

Equipped with the preparatory work reported in the previous sections, we are now ready to discuss our main analysis. We begin by looking for GRB-neutrino candidates, using the data described in section 2. For each GRB-neutrino pair selected by our directional criteria ($\mathcal{S} \geq 1/4\pi$) we describe the Δt of eq. (1.1) as the difference between the neutrino observation time[5] and the observation time of the GRB, which we label as $\Delta t_{\rm candidate}$, and then we use eq. (1.1) and the known redshift of the GRB, which we label as $z_{\rm GRB}$, to convert the requirement that η should be within the interval $[12.7, 30.7]$ into a corresponding range of allowed values for the neutrino energy. We then consider the GRB-neutrino pair a

[4] In the following, whenever we refer to simulated data, it is understood that we did all computations based on 10^5 instances.

[5] If there was no in-vacuo dispersion, a GRB neutrino would be observed (nearly-)simultaneously with the GRB photons. We attribute the whole of the time-of-arrival difference to the Δt of the neutrino, since photons observed from GRBs are of much lower energies than our neutrinos and the effect we are studying depends linearly on energy. Some quantum-spacetime scenarios predict in-vacuo dispersion with different magnitude for photons and neutrinos (and if the magnitude was much stronger for photons this assumption of our analysis would not be satisfied); it is however noteworthy that effective-field-theory approaches to quantum properties of spacetime predict that the type of pure in-vacuo dispersion here studied is actually forbidden for photons whereas it is allowed for neutrinos [17, 49].

JCAP02(2026)035

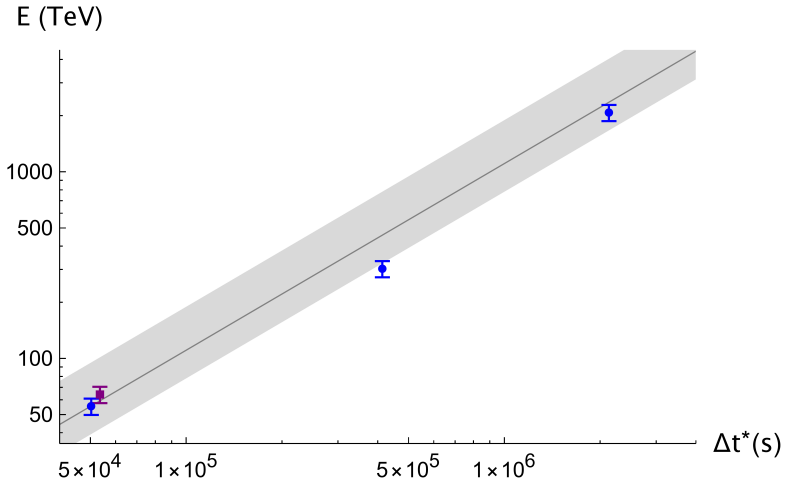

Figure 1. The values of E and Δt^* of our four GRB-neutrino candidates line up rather nicely according to the expectations of in-vacuo dispersion. Only one of them, here shown as a violet square, was taken into account also in the analysis of ref. [32]. The content of this figure should be assessed also keeping in mind the results here reported in section 3, suggesting that it is likely that one of our four GRB-neutrino candidates is background. Based on the estimate $\eta = 21.7 \pm 4.5$ reported in ref. [32], the dark-gray line corresponds to $\eta = 21.7$, while the light-gray band highlights our region of interest in the E-Δt^* plane, corresponding to $\eta \in [12.7, 30.7]$ via eq. (1.1) (see section 1 for comments on this interval).

GRB-neutrino candidate if the energy of the neutrino is compatible with that energy range within two standard deviations (assuming 10% uncertainty in the energy of the neutrino [39]). We find that there are four such GRB-neutrino candidates. Figure 1 provides a visual characterization of the fact that the properties of these four GRB-neutrino candidates match rather well the expectations of the in-vacuo-dispersion scenario of eq. (1.1).

In figure 1, the rescaled time delay Δt^* is defined as

$$\Delta t^* \equiv \frac{D(1)}{D(z_{\rm GRB})} \Delta t_{\rm candidate} \tag{4.1}$$

(the numerical factor $D(1)$ is introduced only for the convenience of having a Δt^* with dimensions of time), and according to eq. (1.1) one should find a linear relationship between E and Δt^*,

$$\Delta t^* = \eta D(1) \frac{E}{M_P} \,. \tag{4.2}$$

It is clearly encouraging for the hypothesis of in-vacuo dispersion that our criteria find four GRB-neutrino candidates (some details on these four GRB-neutrino candidates are provided in appendix B), whereas according to the pure-background null hypothesis we expected to typically find only one (see section 3). Further encouragement comes from the fact that in figure 1 our four GRB-neutrino candidates line up rather nicely, as measured by their correlation coefficient $r(\Delta t^*, E) = 0.9985$. In particular, three of the four GRB-neutrino candidates are compatible with a remarkably narrow range of values of η, an observation

JCAP02(2026)035

which strengthens the appeal of the conjecture that three of our four GRB-neutrino candidates actually might be GRB neutrinos affected by in-vacuo dispersion.

The fact that our findings reported in figure 1 fit very well with the estimate $\eta = 21.7 \pm 4.5$, which resulted from the analysis of ref. [32], is noteworthy since, because of the different criteria adopted for the selection of GRB-neutrino candidates, the two analyses only share one GRB-neutrino candidate, the one shown as a violet square in figure 1. The analysis leading to the estimate $\eta = 21.7 \pm 4.5$, in ref. [32] ended up focusing on seven GRB-neutrino candidates, but only one of them involved a GRB with measured redshift.

It is of course necessary to quantify statistically this observation that the data we are analyzing match well the expectations of in-vacuo dispersion. For this purpose we rely on the same strategy of characterization of statistical significance adopted in ref. [32]. In parts of the next section we shall contemplate alternative strategies of characterization of statistical significance, but the main objective of the study we are here reporting is to compare the GRB-neutrino-candidate selection criteria here adopted with the selection criteria adopted in ref. [32], and this comparison is of course more transparent if the two selection strategies are assessed using the same characterization of statistical significance. The main analysis of ref. [32] focused on seven GRB-neutrino candidates and established how frequently simulated data produced at least seven GRB-neutrino candidates with correlation at least as high as the correlation of the GRB-neutrino candidates found in the true data. This happened in about 0.7% of the trials, yielding the above-mentioned p-value $P_{[34]} = 0.007$. Proceeding in an analogous way with the selection criteria here adopted, we start by using our simulated data (section 3) to estimate how frequently the null hypothesis of no in-vacuo dispersion ($\eta = 0$) would produce at least four GRB-neutrino candidates according to our new selection criteria, finding a p-value $P_n = 0.019$. We then proceed to estimate how frequently the null hypothesis would accidentally exhibit at least four GRB-neutrino candidates with correlation $r(\Delta t^*, E) \geq 0.9985$, finding a p-value $P_r = 0.006$ (which corresponds to a 2.8σ significance in Gaussian statistics).

5 Avenues for refining the strategy of analysis

We consider as our main result the p-value $P_r = 0.006$ derived in the previous section, which, while being still far from conclusive, testifies to the discovery potential of the novel GRB-neutrino-candidate selection criteria here advocated, which was our main objective.

In this section we discuss and investigate some observations which could be used to refine the strategy of analysis. We believe that some of the observations reported in this section deserve being considered in setting up in-vacuo-dispersion analyses of future neutrino data, even though some of the quantitative aspects of this section should be assessed with caution since they were produced in a second phase of our investigations after seeing the data, and might therefore be affected by the sources of bias that are well known for unblind analyses. In particular, some of the observations reported in this section are at least in part inspired by the fact that among our four GRB-neutrino candidates there are three that are described particularly well according to eq. (1.1), and by our perception this was not fully taken into account by the procedure used in section 4 to estimate the significance of our findings.

JCAP02(2026)035

5.1 Alternative choices of $S_{\rm cut}$

In planning our study we ended up adopting the rather prudent criterion of directional consistency characterized by the intuitively natural choice $\mathcal{S}_{\rm cut} = 1/4\pi$ (see section 1). After completing our main analysis we perceived the need to quantify how frequently this criterion was picking up accidental directional associations between a neutrino and a GRB. Using our simulated data, we checked that the choice $\mathcal{S}_{\rm cut} = 1/4\pi$ entails a 7.8% probability of accidental directional association between a neutrino and a GRB, which is of course partly responsible for the (large but) tolerable expectation that about one background GRB-neutrino candidate should be accidentally picked up by our overall selection criteria (see section 3).

We then performed a rudimentary investigation of the dependence of the p-value P_r, which we regard as our main result, on the choice of $\mathcal{S}_{\rm cut}$. Taking as starting point the observation that $\mathcal{S}_{\rm cut} = 1/4\pi$ entails a 7.8% probability of accidental directional association, we show in figure 2 the values of P_r obtained by redoing our analysis upon adopting values of $\mathcal{S}_{\rm cut}$ that entail a probability of accidental directional association between 2.7% and 40%. To obtain figure 2 we varied $\mathcal{S}_{\rm cut}$, but we then found most insightful to show in figure 2 directly the dependence of P_r on $\mathcal{S}_{\%}$, denoting with $\mathcal{S}_{\%}$ the percentage probability of accidental directional association found for a given value of $\mathcal{S}_{\rm cut}$.

Several features of figure 2 deserve some comment. We start from observing that figure 2 clearly reflects the "optimization issue" briefly discussed at the end of section 1: of course, for very large values of $\mathcal{S}_{\%}$ one picks up too much noise, while for very low values of $\mathcal{S}_{\%}$ one throws away too much of the signal. In such situations, one expects that there is a certain range of $\mathcal{S}_{\%}$ giving a reasonable balance between keeping most of the signal and not picking up too much noise; and that, within that range, one can find a value of $\mathcal{S}_{\%}$ which optimizes the discovery potential of the statistical approach. Presently available data suggest, as shown in figure 2 and, more visibly, in figure 3, that a reasonable balance is indeed found for a rather wide range of $\mathcal{S}_{\%}$, between 4.5 and 15: for choices of $\mathcal{S}_{\rm cut}$ corresponding to this entire range our analysis would find p-values that remain rather close to the value 0.006 which we quoted as our main result (the maximum value of P_r found in that range is 0.011, while the minimum is 0.0012). Figure 2 and figure 3 also appear to suggest that the optimum could be reached for values of $\mathcal{S}_{\%}$ a bit higher than 7.8 (i.e., for values of $\mathcal{S}_{\rm cut}$ a bit lower than $1/4\pi$), but it would be premature at this stage to orient future studies toward values of $\mathcal{S}_{\rm cut}$ lower than $1/4\pi$: our original choice $\mathcal{S}_{\rm cut} = 1/4\pi$, motivated by the considerations expressed at the end of section 1, performs rather well on presently-available data, and the fact that on presently-available data somewhat lower values of $\mathcal{S}_{\rm cut}$ produce even lower p-values might just be a peculiarity of presently-available data. How the peculiarities of presently-available data can affect this sort of assessments is demonstrated by the "jumps" in P_r occurring at certain specific values of $\mathcal{S}_{\%}$ which can be clearly noticed in figure 2 and figure 3: with the limited number of neutrinos that are presently available for our analysis there can be a strong difference between two close values of $\mathcal{S}_{\%}$ if the higher one picks up an extra GRB-neutrino candidate which does not make the lower cut. When preliminary optimization analyses of the sort we are performing in this subsection display such non-smoothness features, it usually means that much more data is needed to conclusively assess which choices best optimize the discovery potential of the statistical analysis.

JCAP02(2026)035

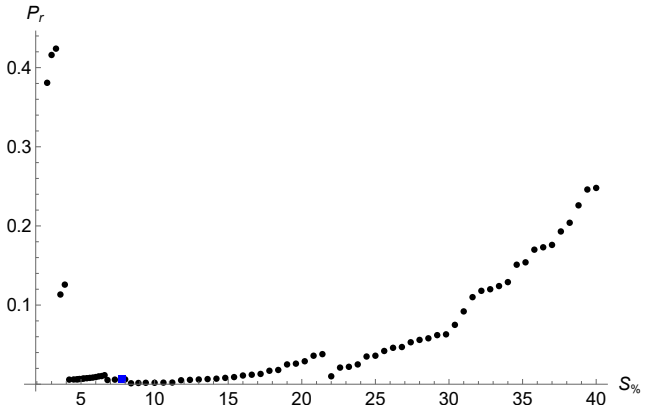

Figure 2. The p-value P_r (see section 4 for the definition) as a function of $\mathcal{S}_{\%}$. The blue square corresponds to the choice $\mathcal{S}_{\rm cut} = 1/4\pi$ of section 4 (which gives $\mathcal{S}_{\%} = 7.8$).

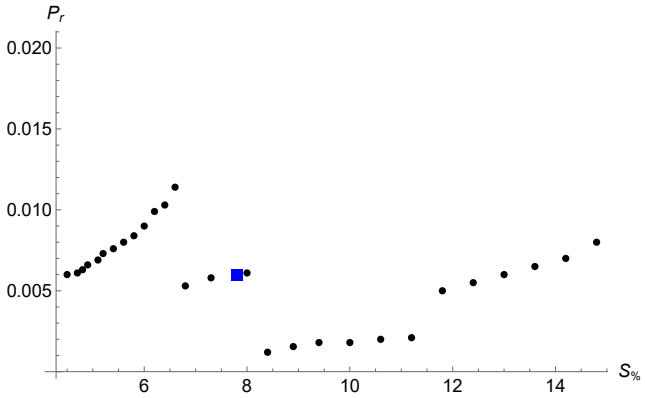

Figure 3. Same as figure 2, but focusing on the range $4.5 \leq \mathcal{S}_{\%} \leq 15$ for a better visualization of some of the most noteworthy features.

5.2 Improved correlation

One challenge whose handling might require further methodological refinements in future studies concerns the choice of an appropriate statistic quantifying the agreement between the properties of the found GRB-neutrino candidates and eq. (1.1). Investigations of this aspect should take into account the fact that the time window for in-vacuo dispersion searches of GRB neutrinos will always be rather large, even if, as one might hope, the η range on which one would focus could become narrower with the accrual of more data. A relatively small uncertainty on η still translates (especially at high neutrino energies and high redshift) into a rather large time window, large enough for a tangible probability of background contamination of the GRB-neutrino candidates. These concerns are even more severe if one allows for non-systematic, fuzzy in-vacuo dispersion effects of the type mentioned here briefly in section 1 (and discussed in more detail in, e.g., refs. [18, 19, 26]), since in that case searches of GRB-neutrino candidates would always have to explore a range of η with width at least $\delta\eta$.

Awareness of these issues should encourage investigations aimed at quantifying the agreement between the found GRB-neutrino candidates and the relevant in-vacuo-dispersion

JCAP02(2026)035

models in ways that are both robust against contamination by the background and capable of profiting from all the implications of in-vacuo-dispersion.

In our main analysis, reported in section 4, we followed ref. [32] and characterized the agreement between our findings and eq. (1.1) in terms of the standard (Pearson) correlation coefficient $r(\Delta t^*, E)$. However, r, while giving an appropriate weight to the linear relationship between E and Δt^* predicted by eq. (1.1), is completely insensitive to the fact that, according to eq. (1.1), one should have $\Delta t^* \to 0$ for $E \to 0$. We observe that this shortcoming can be remedied by replacing the sample covariance and the sample variances appearing in the definition of r with the corresponding raw (non-central) sample moments, i.e., by replacing $r(\Delta t^*, E)$ with the corresponding non-central correlation coefficient

$$r_0(\Delta t^*, E) = \frac{\sum_i \Delta t_i^* E_i}{\sqrt{\sum_j (\Delta t_j^*)^2 \sum_k E_k^2}}.$$

It is clear that r_0 indeed rewards GRB-neutrino candidates fitting the expectation that E depends linearly on Δt^* with negligible intercept.

We can test the effectiveness of this improved statistic by replacing r with r_0 in our main analysis (section 4). Our four GRB-neutrino candidates have $r_0(\Delta t^*, E) = 0.9989$, and requiring that our simulated data (section 3) accidentally produce at least four GRB-neutrino candidates with $r_0(\Delta t^*, E) \geq 0.9989$, we find a p-value $P_{r_0} = 0.004$.

The fact that $P_{r_0} < P_r$ suggests that our GRB-neutrino candidates are indeed consistent with the expectation that $\Delta t^* \to 0$ for $E \to 0$.

5.3 Taking into account the background estimate

Regardless of the statistic used to quantify the agreement of the found GRB-neutrino candidates with eq. (1.1), one could also try to tame background contamination by taking explicitly into account its contribution before computing the statistic.

Looking at the GRB-neutrino candidate with $E = 302\,\text{TeV}$ in figure 1, one can easily understand these concerns: even though we expect that one of our four GRB-neutrino candidates should be background, in our main analysis (following ref. [32]) we computed the correlation coefficient of all of them. Future studies might thus contemplate the possibility of taking into account the background estimate. More explicitly, if one finds N GRB-neutrino candidates and estimates that there is a large probability, e.g., 90%, that at least M should be background, it may be appropriate to assess the agreement between the found GRB-neutrino candidates and eq. (1.1) using only the best $N - M$ candidates.

In the case of the study here reported, the probability of finding at least one background candidate is still too low (about 60%) to justify disregarding our worst candidate. Nevertheless, for mere illustrative purposes, we briefly discuss how to amend our main analysis if one of our four candidates could be actually ignored. First, we compute the correlation coefficients of all possible choices of three of our four GRB-neutrino candidates and find that the highest correlation is $r(\Delta t^*, E) = 0.999997$ (found indeed excluding the candidate with $E = 302\,\text{TeV}$). We then use our simulated data to estimate how frequently the null hypothesis would accidentally produce at least four GRB-neutrino candidates such that three of them have correlation $r(\Delta t^*, E) \geq 0.999997$, finding a p-value $P_{rb} = 0.002$.

JCAP02(2026)035

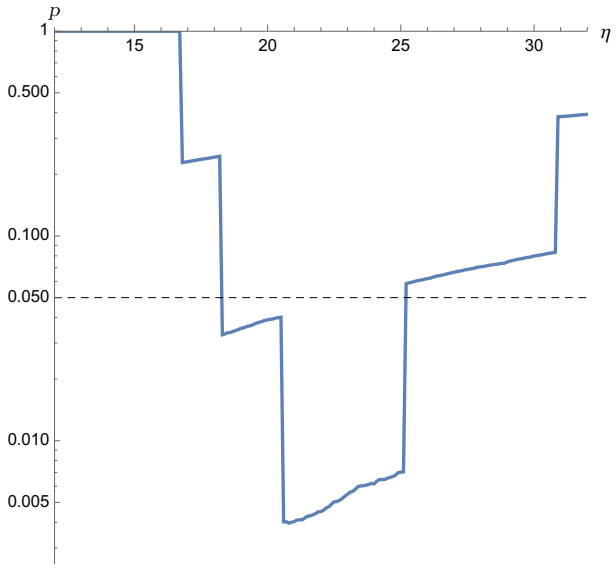

Figure 4. The p-curve for $\eta \in [12.7, 30.7]$. It is obtained estimating how frequently simulated data produce at least the same number of GRB-neutrino candidates as the real data for each value of η (see text for details). The horizontal dashed line is drawn at $p = 0.05$.

5.4 Scanning a range of values of η

The fact that we are restricting our analysis to GRBs with measured redshift allows us to explore another statistic, which we expect to be less vulnerable than correlation to background contamination.

For simplicity we illustrate and discuss the strategy of analysis based on this alternative statistic applying it directly to the data already analyzed in this paper. For every given value of η in our interval of interest $[12.7, 30.7]$, we find the number $N(\eta)$ of GRB-neutrino candidates which are directionally compatible in the usual sense ($\mathcal{S} \geq 1/4\pi$) and satisfy eq. (1.1) for that specific value of η within two standard uncertainties in the neutrino energy. We then use simulated data to estimate the probability that the null hypothesis would accidentally produce at least $N(\eta)$ such GRB-neutrino candidates, finding a corresponding (local) p-value $p(\eta)$. The resulting "p-curve" is reproduced here as figure 4.

Consistently with the fact, already visible in figure 1, that our four GRB-neutrino candidates are remarkably compatible with a narrow range of values of η, we see that the p-curve of figure 4 shows a deep valley surrounded by considerably higher values of p. In particular, $p(\eta)$ is less than 0.05 (marked as a dashed horizontal line in figure 4) for $\eta \in [18.3, 25.1]$. The minimum of the p-curve is found at $\eta = 20.8$, fully consistent with the estimate 21.7 ± 4.5 reported in ref. [32].

The statistical significance of our p-curve can be characterized estimating how frequently the minimum of the analogous p-curves built out of simulated data happens to be less than or equal to the minimum value $p(20.8) = 0.004$ attained in figure 4. The resulting (global) p-value is $P_{ns} = 0.012$.

The fact that P_{ns} and P_r, resulting from considerably different strategies of analysis, are of the same order of magnitude suggests that both values are in fact genuine characterizations

JCAP02(2026)035

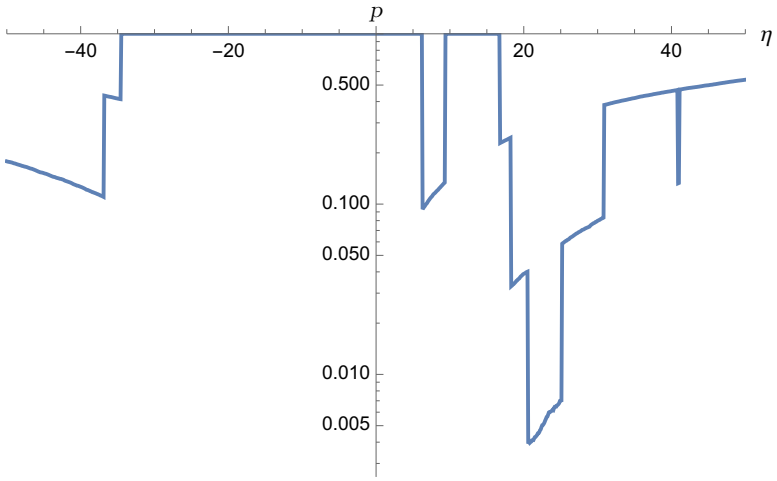

Figure 5. The same p-curve of figure 4 for $\eta \in [-50, 50]$.

of the statistical significance of our results, i.e., that they are not too dependent on the specific properties of the corresponding statistics.

5.5 Exploring η outside the range $[12.7, 30.7]$

In our main analysis we let η vary in the range $[12.7, 30.7]$ favored by the previous study [32], which adopted different selection criteria, obtaining results in remarkable agreement with those of ref. [32]. Still, it is interesting to check whether our new GRB-neutrino-candidate selection criteria would have yielded even stronger results for values of η outside the range $[12.7, 30.7]$. A natural way of doing this is to extend the domain of the p-curve introduced in the previous subsection. In figure 5 we show the p-curve for $\eta \in [-50, 50]$.

Looking at figure 5, it is clear that also our new GRB-neutrino-candidate selection criteria favor the range $[12.7, 30.7]$ for η. The fact that we find no other values of η with comparable $p(\eta)$ is also potentially significant for a much-studied effective-field-theory description of quantum-spacetime properties [49, 50], which in principle allows independent in-vacuo-dispersion parameters for the two neutrino helicities. The prevalent theoretical prejudice is that the two helicities should have the same in-vacuo-dispersion parameter, but it has also been argued that the two helicities might have η with the same modulus but opposite sign [21, 24]. The p-curve reproduced in figure 5 clearly does not provide any encouragement for this helicity-dependence scenario.

6 Outlook

The essential equivalence of the p-values $P_{[34]}$, characterizing the statistical significance of the previous analysis [32], and P_r, found here in section 4 and characterizing in the same way the significance of our current analysis, shows that the new, redshift-based selection criteria for GRB-neutrino candidates proposed in section 1 are competitive with the ones adopted in ref. [32]. This means that the improvement in data quality provided by the knowledge of the GRB redshifts is more than sufficient to compensate for the loss of most of the GRB dataset (we measure the redshift of about 1/10 of observed GRBs). We feel that this is our

JCAP02(2026)035

main result, as it effectively opens up a new avenue, complementary to the approach pursued in ref. [32], to investigate in-vacuo dispersion for neutrinos.

Considering the very significant differences in their selection criteria (as stressed above, only one GRB-neutrino candidate figures in both analyses), it is noteworthy that the analysis here reported and the one reported in ref. [32] both favor the same range of values of η. This might suggest that, if one were somehow able to combine the two analyses, then the overall evidence in favor of in-vacuo dispersion provided by presently-available IceCube data might be stronger than indicated by the individual statistical significance of each analysis. However, we do not yet see how such a combination of selection criteria could be achieved in a logically consistent manner, mostly because sharp knowledge of the GRB redshifts is a structural feature of the strategy of analysis advocated here.

We expect that the redshift-based strategy articulated in the previous sections will prove to be the best starting point for any future refinements, but we do not exclude that a suitable way may still be found for including GRBs whose redshift has not been measured (of course, from the perspective of our approach, somehow estimating the redshift of those GRBs with a suitably large uncertainty). Such a refinement of our approach could prove even more valuable in a few years, as more IceCube and KM3NeT data is accrued.

At least equally important for the analysis of future IceCube and KM3NeT data would be to remove the other key limitation of our selection criteria, the restriction to shower-event neutrinos. This could in principle be achieved by incorporating into the analysis the known [40] large and non-Gaussian probability distribution (whose peak lies sizably above the visible energy) that relates the primary neutrino energy to the visible energy in track events.

Acknowledgments

We thank Anastasia Tsvetkova for guidance on the available GRB catalogues and resources, which was very valuable in the early stages of our work on appendix A. G.A.-C. and G.G. are grateful for financial support by the Programme STAR Plus, funded by Federico II University and Compagnia di San Paolo, and by the MIUR, PRIN 2017 grant 20179ZF5KS. G.R.'s work on this project was supported by the National Science Centre grant 2019/33/B/ST2/00050. G.D.'s work on this project was supported by the Research Council of Norway, project number 301718, and by the Beatriu de Pinós programme (BP 2023). G.F.'s work on this project was supported by "Fondazione Angelo Della Riccia" and "The Foundation Blanceflor". This work also falls within the scopes of the COST Action CA23130 "Bridging high and low energies in search of quantum gravity" and the COST Action CA18108 "Quantum Gravity phenomenology in the Multi-Messenger era".

A Known-redshift GRB data

The following table contains the GRB data used in our analysis. We include all GRBs observed up to December 2022 for which a definite redshift determination is available in the literature. We did not include GRBs with only upper and/or lower bounds on redshift. For the selection of the sample and the redshift values z we relied mostly on Greiner's catalogue [43], referred to in our list as MP. Searching the literature for other GRBs whose redshift was measured, we

JCAP02(2026)035

found 45 which are not acknowledged as such in the summary table of [43]. For these GRBs we provide references to the relevant works and GCNs in the column "z ref." of our table.

The angular data and the trigger times (TT) of the GRBs in our sample were downloaded from the web catalogue maintained by the IceCube collaboration [42], and were then manually checked against the primary GCN sources referred to in Greiner's list [43]. If the right ascension (RA) or the declination (decl) values reported by [42] were no more than 0.001° off the best values we found in [43], we did not correct them, as our analysis is completely insensitive to errors of that order of magnitude. For the same reason, we do not provide the uncertainties affecting the angular positions, since we checked that they are all less than 0.001°. Accordingly, we report our angular values with three digital figures, with the understanding that the last one is affected by an uncertainty of order 0.001°.

Name	RA (°)	decl (°)	TT (MJD)	z	z ref.
GRB221226B	22.909	−41.527	59939.945	2.694	MP
GRB221110A	29.100	−27.294	59893.103	4.06	MP
GRB221009A	288.264	19.773	59861.553	0.151	MP
GRB221006A	337.246	15.714	59858.040	0.731	[51, 52]
GRB220813A	81.532	−33.016	59804.808	0.82	[53]
GRB220627A	201.369	−32.426	59757.890	3.084	MP
GRB220611A	66.515	−37.260	59741.751	2.3608	MP
GRB220527A	323.528	−14.972	59726.387	0.857	MP
GRB220521A	275.230	10.372	59720.972	5.6	MP
GRB220219B	240.914	31.234	59629.394	0.293	MP
GRB220117A	91.572	−28.437	59596.680	4.961	MP
GRB220107A	169.807	34.171	59586.615	1.246	MP
GRB220101A	1.353	31.769	59580.215	4.618	MP
GRB211227A	132.149	−2.735	59575.981	0.228	[54, 55]
GRB211211A	212.292	27.889	59559.549	0.073	[56, 57]
GRB211207A	149.624	−24.359	59555.870	2.272	MP
GRB211024B	154.713	24.568	59511.931	1.1137	MP
GRB211023B	170.310	39.136	59510.879	0.862	MP
GRB211023A	73.154	85.324	59510.546	0.39	MP
GRB210919A	80.254	1.312	59476.020	0.2411	MP
GRB210905A	309.048	−44.440	59462.009	6.318	MP
GRB210822A	304.438	5.283	59448.388	1.736	MP
GRB210731A	300.305	−28.061	59426.931	1.2525	MP
GRB210722A	27.030	−6.347	59417.871	1.145	MP
GRB210702A	168.578	−36.747	59397.797	1.16	MP
GRB210619B	319.718	33.850	59385.000	1.937	MP
GRB210610B	243.918	14.399	59375.827	1.13	MP
GRB210610A	204.282	14.465	59375.628	3.54	MP
GRB210517A	358.224	−39.102	59351.228	2.486	MP

Table 1. List of GRBs with measured redshift.

JCAP02(2026)035

Name	RA (°)	decl (°)	TT (MJD)	z	z ref.
GRB210504A	222.392	−30.534	59338.580	2.077	MP
GRB210420B	254.325	42.570	59324.774	1.4	MP
GRB210411C	296.612	−39.398	59315.629	2.826	MP
GRB210323A	317.947	25.369	59296.918	0.733	MP
GRB210321A	87.895	70.130	59294.301	1.487	MP
GRB210312B	155.814	76.869	59285.870	1.069	MP
GRB210222B	154.606	−14.932	59267.943	2.198	MP
GRB210210A	262.771	14.663	59255.084	0.715	MP
GRB210204A	117.081	11.410	59249.270	0.876	MP
GRB210116A	123.814	−5.867	59230.246	2.514	MP
GRB210112A	219.006	33.054	59226.067	2	[58, 59]
GRB210104A	103.772	64.676	59218.477	0.46	MP
GRB201221D	171.059	42.144	59204.963	1.045	MP
GRB201221A	214.480	−45.416	59204.298	5.7	MP
GRB201216C	16.370	16.516	59199.963	1.1	MP
GRB201104B	5.215	7.842	59157.732	1.954	MP
GRB201103B	42.185	12.137	59156.755	1.105	MP
GRB201024A	125.952	3.354	59146.117	0.999	MP
GRB201021C	12.529	−55.866	59143.852	1.07	MP
GRB201020B	75.470	77.068	59142.732	0.804	MP
GRB201020A	261.228	31.428	59142.241	2.903	MP
GRB201015A	354.319	53.416	59137.952	0.426	MP
GRB201014A	20.796	27.660	59136.950	4.56	MP
GRB200829A	251.205	72.329	59090.582	1.25	MP
GRB200826A	6.786	34.027	59087.187	0.7481	MP
GRB200613A	153.042	45.754	59013.229	1.227	MP
GRB200524A	213.043	60.905	58993.211	1.256	MP
GRB200522A	5.682	−0.283	58991.487	0.554	MP
GRB200411A	47.664	−52.318	58950.187	0.7	MP
GRB200219A	342.638	−59.120	58898.317	0.48	MP
GRB200205B	107.788	−56.488	58884.807	1.465	MP
GRB191221B	154.830	−38.158	58838.861	1.148	MP
GRB191031D	283.289	47.644	58787.891	0.5	MP
GRB191019A	340.025	−17.328	58775.634	0.248	MP
GRB191011A	44.728	−27.845	58767.192	1.722	MP
GRB191004B	49.205	−39.634	58760.898	3.503	MP
GRB190919B	311.877	−44.695	58745.991	3.225	MP
GRB190829A	44.544	−8.958	58724.830	0.0785	MP
GRB190719C	240.207	13.000	58683.624	2.469	MP
GRB190627A	244.828	−5.289	58661.471	1.942	MP

Table 1. List of GRBs with measured redshift.

JCAP02(2026)035

Name	RA (°)	decl (°)	TT (MJD)	z	z ref.
GRB190613A	182.529	67.235	58647.172	2.78	MP
GRB190324A	49.616	−47.215	58566.947	1.1715	MP
GRB190114C	54.505	−26.946	58497.873	0.425	MP
GRB190114A	65.544	2.192	58497.133	3.3765	MP
GRB190106A	29.880	23.846	58489.566	1.859	MP
GRB181201A	319.297	−12.631	58453.110	0.45	[60, 61]
GRB181123B	184.367	14.598	58445.231	1.754	MP
GRB181110A	302.318	−36.897	58432.364	1.505	MP
GRB181020A	13.982	−47.381	58411.792	2.938	MP
GRB181010A	52.570	−23.038	58401.247	1.39	MP
GRB180914B	332.356	25.062	58375.766	1.096	MP
GRB180805B	25.782	−17.494	58335.543	0.661	MP
GRB180728A	253.565	−54.044	58327.728	0.117	MP
GRB180727A	346.666	−63.052	58326.594	2	MP
GRB180720B	0.529	−2.919	58319.598	0.654	MP
GRB180703A	6.468	−67.179	58302.876	0.6678	MP
GRB180624A	318.098	−2.338	58293.576	2.855	MP
GRB180620B	357.521	−57.962	58289.660	1.1175	MP
GRB180618A	169.941	73.837	58287.030	0.544	MP
GRB180510B	77.969	−62.324	58248.844	1.305	MP
GRB180418A	170.122	24.933	58226.281	1.55	MP
GRB180404A	83.548	−37.168	58212.032	1	MP
GRB180329B	82.904	−23.690	58206.589	1.998	MP
GRB180325A	157.428	24.464	58202.078	2.248	MP
GRB180314A	99.265	−24.496	58191.030	1.445	MP
GRB180205A	126.820	11.542	58154.184	1.409	MP
GRB180115A	12.039	−15.630	58133.178	2.487	MP
GRB171222A	148.278	35.627	58109.684	2.409	MP
GRB171205A	167.415	−12.588	58092.306	0.0368	MP
GRB171020A	39.248	15.204	58046.963	1.87	MP
GRB171010A	66.581	−10.463	58036.792	0.3293	MP
GRB170903A	254.526	34.979	57999.534	0.886	MP
GRB170817A	197.450	−23.381	57982.529	0.0098	MP
GRB170728B	237.981	70.122	57962.961	1.27	MP
GRB170728A	58.888	12.182	57962.287	1.49	MP
GRB170714A	34.350	1.991	57948.518	0.793	MP
GRB170705A	191.704	18.307	57939.115	2.01	MP
GRB170607A	7.366	9.243	57911.971	0.557	MP
GRB170604A	342.656	−15.412	57908.798	1.329	MP
GRB170531B	286.884	−16.418	57904.918	2.366	MP

Table 1. List of GRBs with measured redshift.

JCAP02(2026)035

Name	RA (°)	decl (°)	TT (MJD)	z	z ref.
GRB170519A	163.427	25.374	57892.215	0.818	MP
GRB170428A	330.078	26.916	57871.384	0.454	MP
GRB170405A	219.828	−25.243	57848.777	3.51	MP
GRB170214A	256.341	−1.888	57798.649	2.53	MP
GRB170202A	152.514	5.012	57786.769	3.645	MP
GRB170127B	19.977	−30.358	57780.634	2.2	MP
GRB170113A	61.733	−71.943	57766.420	1.968	MP
GRB161219B	91.714	−26.792	57741.784	0.1475	MP
GRB161129A	316.228	32.135	57721.300	0.645	MP
GRB161117A	322.052	−29.614	57709.066	1.549	MP
GRB161108A	180.788	24.868	57700.148	1.159	MP
GRB161104A	77.894	−51.460	57696.404	0.79	MP
GRB161023A	311.022	−47.663	57684.944	2.708	MP
GRB161017A	142.769	43.127	57678.744	2.013	MP
GRB161014A	332.648	7.469	57675.522	2.823	MP
GRB161001A	71.920	−57.261	57662.045	0.67	MP
GRB160821B	279.977	62.392	57621.937	0.16	MP
GRB160804A	221.630	9.999	57604.064	0.736	MP
GRB160629A	4.863	76.967	57568.930	3.332	MP
GRB160625B	308.598	6.919	57564.945	1.406	MP
GRB160624A	330.193	29.644	57563.477	0.483	MP
GRB160623A	315.298	42.221	57562.208	0.367	MP
GRB160509A	311.754	76.108	57517.374	1.17	MP
GRB160425A	280.327	−54.360	57503.977	0.555	MP
GRB160410A	150.685	3.478	57488.215	1.717	MP
GRB160408A	122.625	71.128	57486.268	1.9	MP
GRB160327A	146.702	54.013	57474.386	5	MP
GRB160314A	112.790	17.000	57461.481	0.726	MP
GRB160303A	168.701	22.742	57450.455	1	MP
GRB160228A	107.316	26.932	57446.732	1.64	MP
GRB160227A	194.808	78.679	57445.814	2.38	MP
GRB160203A	161.951	−24.789	57421.092	3.52	MP
GRB160131A	78.168	−7.050	57418.348	0.971	MP
GRB160121A	109.088	−23.592	57408.577	1.96	MP
GRB160117B	132.195	−16.367	57404.583	0.87	MP
GRB151229A	329.370	−20.732	57385.285	1.4	MP
GRB151215A	93.584	35.516	57371.126	2.59	MP
GRB151112A	2.054	−61.663	57338.573	4.1	MP
GRB151111A	56.845	−44.161	57337.356	3.5	MP
GRB151031A	83.196	−39.122	57326.243	1.167	MP

Table 1. List of GRBs with measured redshift.

JCAP02(2026)035

Name	RA (°)	decl (°)	TT (MJD)	z	z ref.
GRB151029A	38.528	−35.386	57324.326	1.423	MP
GRB151027B	76.220	−6.450	57322.945	4.063	MP
GRB151027A	272.487	61.353	57322.166	0.81	MP
GRB151021A	337.644	−33.197	57316.062	2.33	MP
GRB150915A	319.658	−34.914	57280.888	1.968	MP
GRB150910A	5.667	33.473	57275.378	1.359	MP
GRB150831A	221.024	−25.635	57265.440	1.18	MP
GRB150821A	341.913	−57.894	57255.406	0.755	MP
GRB150818A	230.356	68.342	57252.484	0.282	MP
GRB150728A	292.229	33.916	57231.536	0.46	MP
GRB150727A	203.969	−18.325	57230.793	0.313	MP
GRB150616A	314.717	−53.394	57189.951	1.188	[62]
GRB150518A	234.201	16.330	57160.904	0.256	MP
GRB150514A	74.876	−60.968	57156.774	0.807	MP
GRB150424A	152.306	−26.631	57136.321	1	[63, 64]
GRB150423A	221.579	12.284	57135.269	1.394	MP
GRB150413A	190.425	71.841	57125.580	3.139	MP
GRB150403A	311.505	−62.711	57115.913	2.06	MP
GRB150323A	128.178	45.465	57104.118	0.593	MP
GRB150314A	126.670	63.834	57095.205	1.758	MP
GRB150301B	89.166	−57.970	57082.818	1.5169	MP
GRB150206A	10.074	−63.182	57059.604	2.087	MP
GRB150120B	39.291	8.078	57042.307	3.5	MP
GRB150120A	10.319	33.995	57042.123	0.46	MP
GRB150101B	188.020	−10.934	57023.641	0.134	MP
GRB141225A	138.779	33.792	57016.959	0.915	MP
GRB141221A	198.287	8.205	57012.338	1.452	MP
GRB141220A	195.066	32.146	57011.252	1.3195	MP
GRB141212A	39.125	18.147	57003.510	0.596	MP
GRB141121A	122.669	22.217	56982.150	1.47	MP
GRB141109A	144.531	−0.608	56970.243	2.993	MP
GRB141028A	322.602	−0.231	56958.455	2.33	MP
GRB141026A	44.084	26.928	56956.109	3.35	MP
GRB141004A	76.734	12.820	56934.973	0.573	MP
GRB140930B	6.348	24.295	56930.821	1.465	MP
GRB140907A	48.146	46.605	56907.672	1.21	MP
GRB140903A	238.014	27.603	56903.625	0.351	MP
GRB140808A	221.222	49.215	56877.037	3.29	MP
GRB140801A	44.069	30.938	56870.792	1.32	MP
GRB140713A	281.106	59.634	56851.780	0.935	MP

Table 1. List of GRBs with measured redshift.

JCAP02(2026)035

Name	RA (°)	decl (°)	TT (MJD)	z	z ref.
GRB140710A	41.068	35.499	56848.428	0.558	MP
GRB140703A	12.996	45.102	56841.026	3.14	MP
GRB140629A	248.977	41.877	56837.595	2.275	MP
GRB140623A	225.473	81.191	56831.223	1.92	MP
GRB140622A	317.173	−14.419	56830.400	0.959	MP
GRB140620A	281.871	49.731	56828.219	2.04	MP
GRB140614A	231.169	−79.129	56822.045	4.233	MP
GRB140606B	328.125	32.015	56814.133	0.384	MP
GRB140518A	227.252	42.418	56795.387	4.707	MP
GRB140515A	186.064	15.105	56792.384	6.32	MP
GRB140512A	289.370	−15.094	56789.814	0.725	MP
GRB140509A	46.594	−62.639	56786.099	2.4	MP
GRB140508A	255.466	46.780	56785.128	1.027	MP
GRB140506A	276.775	−55.636	56783.880	0.889	MP
GRB140430A	102.936	23.024	56777.857	1.6	MP
GRB140428A	194.368	28.385	56775.945	4.7	MP
GRB140423A	197.286	49.842	56770.355	3.26	MP
GRB140419A	126.990	46.240	56766.171	3.956	MP
GRB140331A	134.864	2.717	56747.243	1	[65]
GRB140318A	184.089	20.209	56734.006	1.02	MP
GRB140311A	209.305	0.642	56727.879	4.954	MP
GRB140304A	30.643	33.474	56720.557	5.283	MP
GRB140301A	69.558	−34.257	56717.642	1.416	MP
GRB140226A	221.492	14.993	56714.419	1.98	MP
GRB140213A	105.155	−73.137	56701.807	1.2076	MP
GRB140206A	145.334	66.761	56694.304	2.73	MP
GRB140129B	326.757	26.206	56686.536	0.43	MP
GRB140114A	188.522	27.951	56671.498	3	MP
GRB131231A	10.590	−1.653	56657.198	0.642	MP
GRB131229A	85.232	−4.396	56655.277	1	MP
GRB131227A	67.378	28.883	56653.198	5.3	MP
GRB131117A	332.331	−31.762	56613.024	4.042	MP
GRB131108A	156.502	9.662	56604.862	2.4	MP
GRB131105A	70.967	−62.995	56601.087	1.686	MP
GRB131103A	348.919	−44.640	56599.922	0.599	MP
GRB131030A	345.067	−5.368	56595.872	1.295	MP
GRB131011A	32.526	−4.411	56576.741	1.874	MP
GRB131004A	296.113	−2.958	56569.904	0.717	MP
GRB130925A	41.179	−26.153	56560.164	0.347	MP
GRB130907A	215.892	45.608	56542.902	1.238	MP

Table 1. List of GRBs with measured redshift.

JCAP02(2026)035

Name	RA (°)	decl (°)	TT (MJD)	z	z ref.
GRB130831A	358.624	29.430	56535.545	0.4791	MP
GRB130822A	27.922	−3.208	56526.663	0.154	MP
GRB130716A	179.574	63.053	56489.442	2.2	MP
GRB130702A	217.312	15.774	56475.004	0.145	MP
GRB130701A	357.229	36.100	56474.179	1.155	MP
GRB130615A	274.829	−68.161	56458.406	2.9	[62, 66]
GRB130612A	259.794	16.720	56455.141	2.006	MP
GRB130610A	224.420	28.207	56453.133	2.092	MP
GRB130606A	249.396	29.796	56449.878	5.913	MP
GRB130604A	250.187	68.226	56447.288	1.06	MP
GRB130603B	172.201	17.071	56446.659	0.356	MP
GRB130528A	139.505	87.301	56440.695	1.25	[67]
GRB130518A	355.668	47.465	56430.580	2.489	MP
GRB130515A	283.440	−54.279	56427.056	0.8	MP
GRB130514A	296.283	−7.976	56426.301	3.6	MP
GRB130511A	196.646	18.710	56423.480	1.3033	MP
GRB130505A	137.061	17.485	56417.349	2.27	MP
GRB130427B	314.898	−22.546	56409.556	2.78	MP
GRB130427A	173.137	27.699	56409.324	0.34	MP
GRB130420A	196.106	59.424	56402.311	1.297	MP
GRB130418A	149.037	13.667	56400.792	1.218	MP
GRB130408A	134.405	−32.361	56390.911	3.758	MP
GRB130215A	43.503	13.395	56338.063	0.597	MP
GRB130131B	173.956	15.038	56323.799	2.539	MP
GRB130131A	171.127	48.076	56323.581	1.55	MP
GRB121229A	190.101	−50.594	56290.209	2.707	MP
GRB121226A	168.642	−30.406	56287.798	1.37	MP
GRB121217A	153.710	−62.351	56278.303	3.1	[68]
GRB121211A	195.533	30.148	56272.574	1.023	MP
GRB121209A	326.787	−8.235	56270.916	2.1	MP
GRB121201A	13.467	−42.943	56262.518	3.385	MP
GRB121128A	300.600	54.300	56259.212	2.2	MP
GRB121123A	307.318	−11.860	56254.419	2.7	[69, 70]
GRB121027A	63.598	−58.830	56227.314	1.773	MP
GRB121024A	70.472	−12.291	56224.122	2.298	MP
GRB120923A	303.795	6.221	56193.220	7.8	MP
GRB120922A	234.748	−20.182	56192.938	3.1	MP
GRB120909A	275.736	−59.449	56179.070	3.93	MP
GRB120907A	74.750	−9.315	56177.017	0.97	MP
GRB120815A	273.958	−52.131	56154.093	2.358	MP

Table 1. List of GRBs with measured redshift.

JCAP02(2026)035

Name	RA (°)	decl (°)	TT (MJD)	z	z ref.
GRB120811C	199.683	62.301	56150.649	2.671	MP
GRB120805A	216.538	5.825	56144.895	3.1	MP
GRB120804A	233.948	−28.782	56143.038	1.05	MP
GRB120802A	44.843	13.768	56141.334	3.796	MP
GRB120729A	13.074	49.940	56137.456	0.8	MP
GRB120724A	245.181	3.508	56132.277	1.48	MP
GRB120722A	230.497	13.251	56130.537	0.9586	MP
GRB120716A	313.051	9.599	56124.712	2.486	MP
GRB120714B	355.409	−46.184	56122.888	0.3984	MP
GRB120712A	169.588	−20.034	56120.571	4.1745	MP
GRB120711A	94.678	−70.999	56119.114	1.405	MP
GRB120630A	352.296	42.556	56108.971	0.6	MP
GRB120624B	170.885	8.929	56102.930	2.1974	MP
GRB120521C	214.286	42.145	56068.974	6	MP
GRB120422A	136.910	14.019	56039.300	0.283	MP
GRB120404A	235.010	12.885	56021.535	2.876	MP
GRB120401A	58.082	−17.636	56018.225	4.5	[71]
GRB120327A	246.864	−29.415	56013.122	2.813	MP
GRB120326A	273.905	69.260	56012.056	1.798	MP
GRB120311A	273.092	14.296	55997.232	0.35	[62]
GRB120305A	47.536	28.492	55991.818	0.225	MP
GRB120224A	40.942	−17.761	55981.194	1.1	MP
GRB120211A	87.754	−24.775	55968.499	2.4	MP
GRB120119A	120.029	−9.082	55945.170	1.728	MP
GRB120118B	124.871	−7.185	55944.709	2.943	MP
GRB111229A	76.287	−84.711	55924.943	1.3805	MP
GRB111228A	150.067	18.298	55923.656	0.714	MP
GRB111225A	13.155	51.572	55920.160	0.297	MP
GRB111215A	349.556	32.494	55910.586	2.06	MP
GRB111211A	153.090	11.208	55906.929	0.478	MP
GRB111209A	14.344	−46.801	55904.300	0.677	MP
GRB111129A	307.434	−52.713	55894.679	1.0796	MP
GRB111123A	154.846	−20.645	55888.759	3.1516	MP
GRB111117A	12.693	23.011	55882.510	2.211	MP
GRB111107A	129.478	−66.520	55872.035	2.893	MP
GRB111008A	60.451	−32.709	55842.926	4.9898	MP
GRB111005A	223.282	−19.737	55839.337	0.0131	MP
GRB110918A	32.539	−27.105	55822.894	0.982	MP
GRB110818A	317.337	−63.981	55791.860	3.36	MP
GRB110808A	57.268	−44.194	55781.263	1.348	MP

Table 1. List of GRBs with measured redshift.

Name	RA (°)	decl (°)	TT (MJD)	z	z ref.
GRB110801A	89.437	80.956	55774.826	1.858	MP
GRB110731A	280.504	−28.537	55773.465	2.83	MP
GRB110721A	333.659	−38.593	55763.200	0.382	[62, 72]
GRB110715A	237.684	−46.235	55757.551	0.82	MP
GRB110709B	164.654	−23.455	55751.898	2.109	MP
GRB110503A	132.776	52.208	55684.733	1.613	MP
GRB110422A	112.046	75.107	55673.654	1.77	MP
GRB110402A	197.402	61.253	55653.009	0.854	MP
GRB110213B	41.756	1.146	55605.605	1.083	MP
GRB110213A	42.964	49.273	55605.220	1.46	MP
GRB110205A	164.630	67.525	55597.085	2.22	MP
GRB110128A	193.896	28.065	55589.073	2.339	MP
GRB110106B	134.154	47.003	55567.893	0.618	MP
GRB110106A	79.306	64.174	55567.643	0.093	[73]
GRB101225A	0.198	44.600	55555.776	0.847	MP
GRB101224A	285.924	45.714	55554.227	0.4536	MP
GRB101219B	12.231	−34.566	55549.686	0.5519	MP
GRB101219A	74.585	−2.540	55549.105	0.718	MP
GRB101213A	241.314	21.897	55543.451	0.414	MP
GRB100906A	28.684	55.630	55445.576	1.727	MP
GRB100905A	31.550	14.930	55444.631	7.9	MP
GRB100902A	48.629	30.979	55441.814	4.5	[74]
GRB100901A	27.264	22.759	55440.565	1.408	MP
GRB100816A	351.740	26.578	55424.026	0.8035	MP
GRB100814A	22.473	−17.995	55422.160	1.44	MP
GRB100805A	299.876	52.628	55413.186	1.85	[75]
GRB100728B	44.056	0.281	55405.439	2.106	MP
GRB100728A	88.758	−15.256	55405.095	1.567	MP
GRB100724A	194.543	−11.103	55401.029	1.288	MP
GRB100704A	133.642	−24.203	55381.149	3.6	[76]
GRB100628A	225.973	−31.664	55375.345	0.102	[77, 78]
GRB100625A	15.796	−39.088	55372.773	0.452	MP
GRB100621A	315.305	−51.106	55368.127	0.542	MP
GRB100615A	177.205	−19.481	55362.083	1.398	MP
GRB100606A	350.627	−66.241	55353.800	1.5545	[79]
GRB100518A	304.789	−24.554	55334.482	4	MP
GRB100513A	169.612	3.628	55329.088	4.772	MP
GRB100508A	76.246	−20.711	55324.389	0.5201	MP
GRB100425A	299.196	−26.431	55311.119	1.755	MP
GRB100424A	209.448	1.538	55310.689	2.465	MP

Table 1. List of GRBs with measured redshift.

JCAP02(2026)035

Name	RA (°)	decl (°)	TT (MJD)	z	z ref.
GRB100418A	256.362	11.462	55304.882	0.6235	MP
GRB100414A	192.112	8.693	55300.097	1.368	MP
GRB100413A	266.221	15.834	55299.732	3.9	[80]
GRB100316D	107.628	−56.256	55271.531	0.059	MP
GRB100316B	163.488	−45.473	55271.334	1.18	MP
GRB100316A	251.978	71.827	55271.099	3.155	MP
GRB100302A	195.516	74.590	55257.829	4.813	MP
GRB100219A	154.202	−12.566	55246.636	4.6667	MP
GRB100216A	154.251	35.522	55243.422	0.038	[81, 82]
GRB100213B	124.282	43.448	55240.957	0.604	[83, 84]
GRB100206A	47.163	13.157	55233.563	0.4068	MP
GRB100117A	11.269	−1.595	55213.879	0.92	MP
GRB091208B	29.392	16.890	55173.410	1.063	MP
GRB091127	36.583	−18.952	55162.976	0.49	MP
GRB091109	309.258	−44.158	55144.207	3.076	MP
GRB091029	60.178	−55.956	55133.162	2.752	MP
GRB091024	339.248	56.890	55128.372	1.092	MP
GRB091020	175.730	50.978	55124.900	1.71	MP
GRB091018	32.186	−57.548	55122.867	0.971	MP
GRB091003	251.520	36.625	55107.191	0.8969	MP
GRB090927	343.972	−70.980	55101.422	1.37	MP
GRB090926B	46.308	−39.006	55100.914	1.24	MP
GRB090926	353.400	−66.324	55100.181	2.1062	MP
GRB090902B	264.939	27.324	55076.462	1.822	MP
GRB090814	239.610	25.631	55057.036	0.696	MP
GRB090812	353.202	−10.605	55055.251	2.452	MP
GRB090809	328.680	−0.084	55052.730	2.737	MP
GRB090726	248.680	72.884	55038.946	2.71	MP
GRB090715B	251.340	44.839	55027.877	3	MP
GRB090709	289.927	60.728	55021.319	1.8	[85]
GRB090618	293.994	78.357	55000.353	0.54	MP
GRB090530	179.419	26.594	54981.138	1.266	MP
GRB090529	212.469	24.459	54980.592	2.625	MP
GRB090519	142.279	0.180	54970.881	3.85	MP
GRB090516	138.260	−11.854	54967.352	4.109	MP
GRB090515	164.152	14.441	54966.198	0.403	[86, 87]
GRB090510	333.552	−26.583	54961.016	0.903	MP
GRB090429B	210.667	32.170	54950.229	9.4	MP
GRB090426	189.075	32.986	54947.534	2.609	MP
GRB090424	189.521	16.838	54945.589	0.544	MP

Table 1. List of GRBs with measured redshift.

JCAP02(2026)035

Name	RA (°)	decl (°)	TT (MJD)	z	z ref.
GRB090423	148.889	18.149	54944.330	8.26	MP
GRB090418	269.313	33.406	54939.464	1.608	MP
GRB090417B	209.694	47.018	54938.639	0.345	MP
GRB090407	68.980	−12.679	54928.436	1.4485	MP
GRB090404	239.240	35.516	54925.664	3	MP
GRB090401B	95.088	−8.972	54922.358	3.1	[75]
GRB090328	90.665	−41.882	54918.401	0.736	MP
GRB090323	190.710	17.053	54913.002	3.57	MP
GRB090313	198.401	8.097	54903.379	3.375	MP
GRB090205	220.911	−27.853	54867.961	4.6497	MP
GRB090201	92.052	−46.590	54863.741	2.1	MP
GRB090113	32.057	33.428	54844.778	1.7493	MP
GRB090102	128.244	33.114	54833.122	1.547	MP
GRB081230	37.331	−25.148	54830.858	2	MP
GRB081228	39.462	30.853	54828.054	3.44	MP
GRB081222	22.740	−34.095	54822.204	2.77	MP
GRB081221	15.793	−24.548	54821.681	2.26	MP
GRB081211B	168.265	53.830	54811.260	0.216	[88]
GRB081210	70.484	−11.257	54810.847	2.0631	MP
GRB081203	233.032	63.521	54803.577	2.05	MP
GRB081121	89.276	−60.603	54791.858	2.512	MP
GRB081118	82.592	−43.301	54788.623	2.58	MP
GRB081109	330.790	−54.711	54779.293	0.9787	MP
GRB081029	346.772	−68.156	54768.072	3.8479	MP
GRB081028	121.895	2.308	54767.017	3.038	MP
GRB081008	279.958	−57.431	54747.832	1.9685	MP
GRB081007	339.960	−40.147	54746.224	0.5295	MP
GRB080928	95.070	−55.200	54737.626	1.692	MP
GRB080916C	119.847	−56.638	54725.009	4.35	MP
GRB080916	336.276	−57.023	54725.406	0.689	MP
GRB080913	65.728	−25.130	54722.283	6.695	MP
GRB080906	228.044	−80.518	54715.565	2.1	MP
GRB080905B	301.741	−62.563	54714.705	2.374	MP
GRB080905	287.674	−18.880	54714.499	0.1218	MP
GRB080825B	209.201	−68.955	54703.741	4.3	MP
GRB080810	356.793	0.320	54688.549	3.35	MP
GRB080805	314.223	−62.445	54683.321	1.505	MP
GRB080804	328.668	−53.185	54682.972	2.2045	MP
GRB080721	224.483	−11.724	54668.434	2.591	MP
GRB080710	8.274	19.502	54657.301	0.845	MP

Table 1. List of GRBs with measured redshift.

JCAP02(2026)035

Name	RA (°)	decl (°)	TT (MJD)	z	z ref.
GRB080707	32.618	33.109	54654.353	1.23	MP
GRB080607	194.947	15.920	54624.255	3.036	MP
GRB080605	262.125	4.016	54622.992	1.6398	MP
GRB080604	236.965	20.558	54621.310	1.416	MP
GRB080603B	176.532	68.061	54620.818	2.69	MP
GRB080603	279.409	62.744	54620.471	1.688	MP
GRB080602	19.176	−9.232	54619.063	1.8204	MP
GRB080520	280.193	−54.992	54606.931	1.545	MP
GRB080517	102.242	50.735	54603.891	0.089	MP
GRB080516	120.642	−26.160	54602.012	3.2	[89]
GRB080515	3.163	32.578	54601.251	2.47	MP
GRB080514B	322.845	0.708	54600.414	1.8	MP
GRB080430	165.311	51.686	54586.828	0.767	MP
GRB080413B	326.144	−19.981	54569.369	1.1	MP
GRB080413	287.299	−27.678	54569.121	2.433	MP
GRB080411	37.980	−71.302	54567.886	1.03	MP
GRB080330	169.269	30.623	54555.154	1.51	MP
GRB080325	277.893	36.524	54550.173	1.78	MP
GRB080319C	258.981	55.392	54544.518	1.95	MP
GRB080319B	217.921	36.302	54544.259	0.937	MP
GRB080319	206.333	44.080	54544.240	2.0265	MP
GRB080310	220.058	−0.175	54535.360	2.42	MP
GRB080210	251.267	13.827	54506.326	2.641	MP
GRB080207	207.512	7.502	54503.896	2.0858	MP
GRB080205	98.253	62.792	54501.330	2.72	MP
GRB080129	105.284	−7.846	54494.255	4.349	MP
GRB080123	338.943	−64.901	54488.182	0.495	MP
GRB071227	58.130	−55.984	54461.843	0.383	MP
GRB071122	276.605	47.075	54426.058	1.14	MP
GRB071117	335.044	−63.443	54421.618	1.331	MP
GRB071112C	39.212	28.371	54416.773	0.823	MP
GRB071031	6.405	−58.060	54404.046	2.692	MP
GRB071028B	354.163	−31.621	54401.114	0.94	[90]
GRB071025	355.071	31.778	54398.173	5.2	MP
GRB071021	340.643	23.718	54394.404	2.452	MP
GRB071020	119.665	32.861	54393.293	2.145	MP
GRB071010B	150.539	45.730	54383.865	0.947	MP
GRB071010	288.060	−32.402	54383.154	0.98	MP
GRB071003	301.851	10.947	54376.320	1.6043	MP
GRB070810	189.963	10.751	54322.092	2.17	MP

Table 1. List of GRBs with measured redshift.

Name	RA (°)	decl (°)	TT (MJD)	z	z ref.
GRB070809	203.770	−22.142	54321.807	0.2187	MP
GRB070802	36.899	−55.528	54314.297	2.45	MP
GRB070724	27.808	−18.594	54305.454	0.457	MP
GRB070721B	33.137	−2.195	54302.440	3.626	MP
GRB070714B	57.843	28.298	54295.208	0.92	MP
GRB070714	42.930	30.243	54295.139	1.58	MP
GRB070612	121.369	37.269	54263.110	0.617	MP
GRB070611	1.992	−29.756	54262.081	2.04	MP
GRB070529	283.742	20.659	54249.534	2.4996	MP
GRB070521	242.661	30.256	54241.286	2.0865	MP
GRB070518	254.199	55.295	54238.602	1.161	MP
GRB070508	312.799	−78.385	54228.179	0.82	[91, 92]
GRB070506	347.218	10.722	54226.233	2.31	MP
GRB070429B	328.015	−38.829	54219.131	0.904	MP
GRB070419B	315.707	−31.264	54209.447	1.9591	MP
GRB070419	182.745	39.925	54209.416	0.97	MP
GRB070411	107.333	1.064	54201.842	2.954	MP
GRB070328	65.115	−34.067	54187.162	2.0627	MP
GRB070318	48.487	−42.946	54177.312	0.836	MP
GRB070306	148.097	10.482	54165.695	1.4965	MP
GRB070224	179.027	−13.330	54155.853	1.9922	MP
GRB070223	153.452	43.134	54154.052	1.6295	MP
GRB070208	197.886	61.965	54139.382	1.165	MP
GRB070129	37.004	11.684	54129.983	2.3384	MP
GRB070125	117.824	31.151	54125.306	1.547	MP
GRB070110	0.913	−52.974	54110.307	2.352	MP
GRB070103	352.558	26.876	54103.866	2.6208	MP
GRB061222B	105.353	−25.860	54091.174	3.355	MP
GRB061222	358.264	46.533	54091.145	2.088	MP
GRB061217	160.413	−21.124	54086.153	0.827	MP
GRB061210	144.522	15.621	54079.514	0.4097	MP
GRB061202	105.525	−74.698	54071.341	2.2543	MP
GRB061201	332.134	−74.580	54070.666	0.111	MP
GRB061126	86.602	64.211	54065.367	1.1588	MP
GRB061121	147.227	−13.195	54060.641	1.314	MP
GRB061110B	323.919	6.876	54049.916	3.44	MP
GRB061110	336.291	−2.258	54049.491	0.758	MP
GRB061021	145.150	−21.952	54029.652	0.3463	MP
GRB061007	46.332	−50.501	54015.422	1.261	MP
GRB061006	111.031	−79.199	54014.699	0.4377	MP

Table 1. List of GRBs with measured redshift.

JCAP02(2026)035

Name	RA (°)	decl (°)	TT (MJD)	z	z ref.
GRB061002	220.347	48.742	54010.044	0.564	[65]
GRB060927	329.550	5.364	54005.589	5.47	MP
GRB060926	263.932	13.038	54004.700	3.204	MP
GRB060923B	238.195	−30.904	54001.485	1.5094	MP
GRB060923	254.617	12.361	54001.217	2.6	[85, 93]
GRB060912	5.284	20.972	53990.580	0.937	MP
GRB060908	31.826	0.342	53986.373	1.8836	MP
GRB060906	40.754	30.362	53984.356	3.6855	MP
GRB060904B	58.211	−0.725	53982.105	0.703	MP
GRB060814	221.339	20.586	53961.960	1.9229	MP
GRB060805	220.931	12.586	53952.200	2.3633	MP
GRB060801	213.006	16.982	53948.511	1.131	MP
GRB060729	95.382	−62.370	53945.800	0.54	MP
GRB060719	18.432	−48.381	53935.285	1.532	MP
GRB060714	227.860	−6.566	53930.633	2.7105	MP
GRB060708	7.808	−33.759	53924.511	1.92	MP
GRB060707	357.080	−17.905	53923.896	3.425	MP
GRB060614	320.884	−53.027	53900.530	0.125	MP
GRB060607	329.710	−22.496	53893.217	3.0749	MP
GRB060605	322.156	−6.059	53891.761	3.773	MP
GRB060604	337.229	−10.916	53890.763	2.1357	MP
GRB060602	149.570	0.304	53888.897	0.787	MP
GRB060526	232.826	0.285	53881.686	3.221	MP
GRB060522	322.937	2.886	53877.091	5.11	MP
GRB060512	195.774	41.191	53867.968	2.1	MP
GRB060510B	239.122	78.570	53865.349	4.94	MP
GRB060510	95.867	−1.163	53865.322	1.2	[75]
GRB060505	331.764	−27.815	53860.275	0.089	MP
GRB060502B	278.938	52.632	53857.725	0.287	MP
GRB060502	240.927	66.601	53857.127	1.51	MP
GRB060418	236.428	−3.639	53843.129	1.4895	MP
GRB060319	176.388	60.011	53813.039	1.172	MP
GRB060306	41.095	−2.148	53800.034	1.559	MP
GRB060223	55.206	−17.130	53789.253	4.41	MP
GRB060218	50.416	16.867	53784.149	0.0331	MP
GRB060210	57.739	27.026	53776.208	3.91	MP
GRB060206	202.931	35.051	53772.199	4.048	MP
GRB060204B	211.812	27.677	53770.607	2.3393	MP
GRB060202	35.846	38.384	53768.362	0.783	MP
GRB060124	77.108	69.741	53759.663	2.296	MP

Table 1. List of GRBs with measured redshift.

JCAP02(2026)035

Name	RA (°)	decl (°)	TT (MJD)	z	z ref.
GRB060123	179.700	45.514	53758.932	0.56	MP
GRB060121	137.466	45.663	53756.933	4.6	[94]
GRB060116	84.693	−5.437	53751.359	6.6	[95]
GRB060115	54.035	17.345	53750.547	3.53	MP
GRB060111	276.205	37.604	53746.183	2.32	MP
GRB051227	125.241	31.925	53731.755	0.8	MP
GRB051221	328.703	16.891	53725.077	0.5468	MP
GRB051210	330.171	−57.614	53714.241	2.5	MP
GRB051117B	85.181	−19.274	53691.558	0.481	MP
GRB051111	348.138	18.375	53685.250	1.5495	MP
GRB051109B	345.460	38.680	53683.361	0.08	MP
GRB051109	330.314	40.823	53683.050	2.346	MP
GRB051022	359.017	19.607	53665.547	0.809	MP
GRB051016B	132.116	13.656	53659.770	0.9364	MP
GRB051008	202.873	42.098	53651.690	2.77	MP
GRB051006	110.809	9.506	53649.855	1.059	MP
GRB051001	350.953	−31.523	53644.466	2.4296	MP
GRB050922C	317.388	−8.758	53635.830	2.198	MP
GRB050922B	5.806	−5.605	53635.626	4.5	MP
GRB050915	81.687	−28.016	53628.474	2.5273	MP
GRB050911	13.657	−38.849	53624.666	0.165	[96, 97]
GRB050908	20.461	−12.955	53621.238	3.344	MP
GRB050904	13.711	14.085	53617.078	6.29	MP
GRB050826	87.756	−2.643	53608.263	0.297	MP
GRB050824	12.234	22.609	53606.967	0.83	MP
GRB050822	51.113	−46.033	53604.159	1.434	MP
GRB050820	337.409	19.560	53602.274	2.612	MP
GRB050819	358.757	24.861	53601.683	2.5043	MP
GRB050814	264.189	46.339	53596.485	5.77	MP
GRB050813	241.989	11.248	53595.281	0.72	[98, 99]
GRB050803	350.658	5.786	53585.801	3.5	MP
GRB050802	219.274	27.787	53584.422	1.71	MP
GRB050801	204.146	−21.928	53583.769	1.38	MP
GRB050730	212.072	−3.772	53581.832	3.9678	MP
GRB050724	246.185	−27.541	53575.524	0.2575	MP
GRB050714B	169.699	−15.547	53565.945	2.4383	MP
GRB050709	345.362	−38.978	53560.942	0.16	MP
GRB050525	278.136	26.339	53515.002	0.606	MP
GRB050509B	189.058	28.984	53499.167	0.2255	MP
GRB050505	141.764	30.273	53495.974	4.27	MP

Table 1. List of GRBs with measured redshift.

JCAP02(2026)035

Name	RA (°)	decl (°)	TT (MJD)	z	z ref.
GRB050502B	142.542	16.997	53492.393	5.2	MP
GRB050502	202.443	42.674	53492.093	3.793	MP
GRB050416	188.478	21.057	53476.462	0.6535	MP
GRB050408	180.573	10.852	53468.683	1.2357	MP
GRB050406	34.468	−50.188	53466.666	2.44	[100]
GRB050401	247.870	2.187	53461.597	2.9	MP
GRB050319	154.200	43.548	53448.397	3.24	MP
GRB050318	49.713	−46.396	53447.656	1.44	MP
GRB050315	306.476	−42.600	53444.875	1.949	MP
GRB050223	271.385	−62.472	53424.131	0.5915	MP
GRB050219	166.412	−40.683	53420.528	0.211	MP
GRB050215B	174.448	40.797	53416.107	2.62	MP
GRB050126	278.113	42.370	53396.501	1.29	MP
GRB041006	13.709	1.235	53284.512	0.716	MP
GRB040924	31.594	16.114	53272.494	0.859	MP
GRB040912	359.226	−1.001	53260.592	1.563	MP
GRB040701	311.943	−40.237	53189.583	0.2146	[101, 102]
GRB031203	120.626	−39.850	52976.918	0.105	MP
GRB030528	256.008	−22.650	52787.544	0.782	MP
GRB030429	183.281	−20.914	52758.446	2.656	MP
GRB030329	161.208	21.522	52727.484	0.1685	MP
GRB030328	182.702	−9.348	52726.473	1.52	MP
GRB030323	166.539	−21.770	52721.915	3.372	MP
GRB030226	173.271	25.898	52696.157	1.986	MP
GRB030115	169.625	15.001	52654.141	2.5	[103]
GRB021211	122.270	6.678	52619.471	1.004	MP
GRB021004	6.745	18.949	52551.504	2.33	MP
GRB020903	342.176	−20.769	52520.421	0.25	MP
GRB020819B	351.840	6.250	52505.623	1.9621	MP
GRB020813	296.658	−19.588	52499.114	1.2545	MP
GRB020405	209.513	−31.373	52369.029	0.69	MP
GRB020305	190.616	−14.303	52338.629	0.2	MP
GRB020127	123.756	36.776	52301.873	1.9	MP
GRB020124	143.211	−11.520	52298.445	3.198	MP
GRB011211	168.825	−21.949	52254.798	2.14	MP
GRB011121	173.606	−76.028	52234.783	0.36	MP
GRB010921	344.000	40.931	52173.219	0.45	MP
GRB010222	223.052	43.018	51962.308	1.477	MP
GRB000926	256.040	51.786	51813.877	2.066	MP
GRB000911	34.681	7.741	51798.302	1.0585	MP

Table 1. List of GRBs with measured redshift.

JCAP02(2026)035

Name	RA (°)	decl (°)	TT (MJD)	z	z ref.
GRB000607	38.496	17.002	51702.101	0.1405	[104]
GRB000418	186.330	20.103	51652.896	1.118	MP
GRB000301C	245.078	29.443	51604.529	2.03	MP
GRB000214	283.613	−66.458	51588.042	0.42	MP
GRB000210	29.815	−40.659	51584.364	0.8463	MP
GRB000131	93.379	−51.944	51574.624	4.5	MP
GRB991216	77.380	11.285	51528.672	1.02	MP
GRB991208	248.473	46.456	51520.192	0.706	MP
GRB990712	337.971	−73.408	51371.323	0.434	MP
GRB990705	77.477	−72.131	51364.668	0.842	MP
GRB990510	204.525	−80.500	51308.367	1.619	MP
GRB990506	178.709	−26.676	51304.475	1.3	MP
GRB990123	231.374	44.758	51201.408	1.6	MP
GRB981226	352.405	−23.932	51173.408	1.11	[105]
GRB980703	359.779	8.585	50997.182	0.966	MP
GRB980613	154.442	71.486	50977.202	1.096	MP
GRB980425	293.725	−52.819	50928.446	0.0085	MP
GRB980329	105.658	38.846	50901.156	3.5	MP
GRB980326	129.143	−18.857	50898.888	1	[106]
GRB971214	179.110	65.200	50796.110	3.42	MP
GRB970828	272.106	59.302	50688.739	0.9578	MP
GRB970508	103.456	79.272	50576.904	0.835	MP
GRB970228	75.488	11.768	50507.124	0.695	MP

Table 1. List of GRBs with measured redshift.

B GRBs relevant for figure 1

In this appendix we describe some properties of the GRB-neutrino events appearing in figure 1.

As already stressed in the main text, our analysis relied on the latest HESE neutrino data release by IceCube [37]. We considered only shower neutrinos, for which the energy is approximately equal to the visible energy [39, 40] (whereas the energy of track neutrinos is poorly known).

The GRBs which we analyzed (also in producing simulated data) are those of our catalogue reported in appendix A. It is worth emphasizing that our catalogue agrees with both [42] and [43] for what concerns the four GRBs relevant for figure 1.

The neutrino with the lowest energy among those relevant for figure 1 has a visible energy of 55.3 TeV and is associated to GRB110503A [107], a long GRB (T90 = 10.0 s) with measured redshift of 1.613 [108, 109].

The violet point in figure 1, which is the one that was already taken into account in the analysis of ref. [32], has a visible energy of 64.0 TeV, and is associated to GRB111229A [110], a long GRB (T90 = 25.4 s) with measured redshift of 1.38 [111].

JCAP02(2026)035

The neutrino with visible energy of 302.2 TeV relevant for figure 1 is associated to GRB120923A [112], a long GRB (T90 = 27.2 s) with measured redshift of 7.8 [113].

The highest-energy neutrino relevant for figure 1 (also known as "big bird" [114]) has visible energy of 2075.0 TeV and is associated with GRB120909A [115], a long GRB (T90 = 112.1 s) with measured redshift of 3.93 [116].

References

[1] IceCube collaboration, *Evidence for High-Energy Extraterrestrial Neutrinos at the IceCube Detector*, *Science* **342** (2013) 1242856 [arXiv:1311.5238] [INSPIRE].

[2] IceCube collaboration, *Evidence for neutrino emission from the nearby active galaxy NGC 1068*, *Science* **378** (2022) 538 [arXiv:2211.09972] [INSPIRE].

[3] IceCube collaboration, *Neutrino emission from the direction of the blazar TXS 0506+056 prior to the IceCube-170922A alert*, *Science* **361** (2018) 147 [arXiv:1807.08794] [INSPIRE].

[4] J. Ellis, N.E. Mavromatos, A.S. Sakharov and E.K. Sarkisyan-Grinbaum, *Limits on Neutrino Lorentz Violation from Multimessenger Observations of TXS 0506+056*, *Phys. Lett. B* **789** (2019) 352 [arXiv:1807.05155] [INSPIRE].

[5] T. Piran, *Gamma-ray bursts: A puzzle being resolved*, *Phys. Rept.* **333** (2000) 529 [astro-ph/9907392] [INSPIRE].

[6] E. Waxman and J.N. Bahcall, *High-energy neutrinos from cosmological gamma-ray burst fireballs*, *Phys. Rev. Lett.* **78** (1997) 2292 [astro-ph/9701231] [INSPIRE].

[7] P. Meszaros, *Theoretical models of gamma-ray bursts*, *AIP Conf. Proc.* **428** (1998) 647 [astro-ph/9711354] [INSPIRE].

[8] D. Guetta et al., *Neutrinos from individual gamma-ray bursts in the BATSE catalog*, *Astropart. Phys.* **20** (2004) 429 [astro-ph/0302524] [INSPIRE].

[9] M. Ahlers, M.C. Gonzalez-Garcia and F. Halzen, *GRBs on probation: testing the UHE CR paradigm with IceCube*, *Astropart. Phys.* **35** (2011) 87 [arXiv:1103.3421] [INSPIRE].

[10] G. Amelino-Camelia et al., *Tests of quantum gravity from observations of gamma-ray bursts*, *Nature* **393** (1998) 763 [astro-ph/9712103] [INSPIRE].

[11] U. Jacob and T. Piran, *Neutrinos from gamma-ray bursts as a tool to explore quantum-gravity-induced Lorentz violation*, *Nature Phys.* **3** (2007) 87 [hep-ph/0607145] [INSPIRE].

[12] G. Amelino-Camelia and L. Smolin, *Prospects for constraining quantum gravity dispersion with near term observations*, *Phys. Rev. D* **80** (2009) 084017 [arXiv:0906.3731] [INSPIRE].

[13] R. Gambini and J. Pullin, *Nonstandard optics from quantum space-time*, *Phys. Rev. D* **59** (1999) 124021 [gr-qc/9809038] [INSPIRE].

[14] J. Alfaro, H.A. Morales-Tecotl and L.F. Urrutia, *Quantum gravity corrections to neutrino propagation*, *Phys. Rev. Lett.* **84** (2000) 2318 [gr-qc/9909079] [INSPIRE].

[15] G. Amelino-Camelia and S. Majid, *Waves on noncommutative space-time and gamma-ray bursts*, *Int. J. Mod. Phys. A* **15** (2000) 4301 [hep-th/9907110] [INSPIRE].

[16] R.C. Myers and M. Pospelov, *Ultraviolet modifications of dispersion relations in effective field theory*, *Phys. Rev. Lett.* **90** (2003) 211601 [hep-ph/0301124] [INSPIRE].

JCAP02(2026)035

[17] D. Mattingly, *Modern tests of Lorentz invariance*, *Living Rev. Rel.* **8** (2005) 5 [gr-qc/0502097] [INSPIRE].

[18] G. Amelino-Camelia, *Quantum-Spacetime Phenomenology*, *Living Rev. Rel.* **16** (2013) 5 [arXiv:0806.0339] [INSPIRE].

[19] A. Addazi et al., *Quantum gravity phenomenology at the dawn of the multi-messenger era — A review*, *Prog. Part. Nucl. Phys.* **125** (2022) 103948 [arXiv:2111.05659] [INSPIRE].

[20] Y. Huang, H. Li and B.-Q. Ma, *Consistent Lorentz violation features from near-TeV IceCube neutrinos*, *Phys. Rev. D* **99** (2019) 123018 [arXiv:1906.07329] [INSPIRE].

[21] G. Amelino-Camelia et al., *IceCube and GRB neutrinos propagating in quantum spacetime*, *Phys. Lett. B* **761** (2016) 318 [arXiv:1605.00496] [INSPIRE].

[22] G. Amelino-Camelia et al., *Quantum-gravity-induced dual lensing and IceCube neutrinos*, *Int. J. Mod. Phys. D* **26** (2017) 1750076 [arXiv:1609.03982] [INSPIRE].

[23] G. Amelino-Camelia, G. D'Amico, G. Rosati and N. Loret, *In-vacuo-dispersion features for GRB neutrinos and photons*, *Nature Astron.* **1** (2017) 0139 [arXiv:1612.02765] [INSPIRE].

[24] Y. Huang and B.-Q. Ma, *Lorentz violation from gamma-ray burst neutrinos*, *Commun. Phys.* **1** (2018) 62 [arXiv:1810.01652] [INSPIRE].

[25] PLANCK collaboration, *Planck 2018 results. VI. Cosmological parameters*, *Astron. Astrophys.* **641** (2020) A6 [*Erratum ibid.* **652** (2021) C4] [arXiv:1807.06209] [INSPIRE].

[26] V. Vasileiou, J. Granot, T. Piran and G. Amelino-Camelia, *A Planck-scale limit on spacetime fuzziness and stochastic Lorentz invariance violation*, *Nature Phys.* **11** (2015) 344 [INSPIRE].

[27] FERMI GBM/LAT collaboration, *A limit on the variation of the speed of light arising from quantum gravity effects*, *Nature* **462** (2009) 331 [arXiv:0908.1832] [INSPIRE].

[28] J.R. Ellis et al., *Probes of Lorentz Violation in Neutrino Propagation*, *Phys. Rev. D* **78** (2008) 033013 [arXiv:0805.0253] [INSPIRE].

[29] H. Sahlmann and T. Thiemann, *Towards the QFT on curved space-time limit of QGR. 1. A General scheme*, *Class. Quant. Grav.* **23** (2006) 867 [gr-qc/0207030] [INSPIRE].

[30] L. Philpott, *Causal Set Phenomenology*, arXiv:1009.1593 [INSPIRE].

[31] G. Amelino-Camelia, D. Guetta and T. Piran, *Icecube Neutrinos and Lorentz Invariance Violation*, *Astrophys. J.* **806** (2015) 269 [INSPIRE].

[32] G. Amelino-Camelia et al., *Could quantum gravity slow down neutrinos?*, *Nature Astron.* **7** (2023) 996 [arXiv:2209.13726] [INSPIRE].

[33] KM3NET collaboration, *Letter of intent for KM3NeT 2.0*, *J. Phys. G* **43** (2016) 084001 [arXiv:1601.07459] [INSPIRE].

[34] ICECUBE-GEN2 collaboration, *IceCube-Gen2: the window to the extreme Universe*, *J. Phys. G* **48** (2021) 060501 [arXiv:2008.04323] [INSPIRE].

[35] T. Yuan, *The 8-parameter Fisher-Bingham distribution on the sphere*, *Comput. Stat.* **36** (2021) 409 [arXiv:1906.08247] [INSPIRE].

[36] LIGO SCIENTIFIC et al. collaborations, *Gravitational Waves and Gamma-rays from a Binary Neutron Star Merger: GW170817 and GRB 170817A*, *Astrophys. J. Lett.* **848** (2017) L13 [arXiv:1710.05834] [INSPIRE].

[37] IceCube Collaboration, *IceCube HESE 12-year data release*, Harvard Dataverse, V2 (2023) [DOI:10.7910/DVN/PZNO2T].

JCAP02(2026)035

[38] IceCube collaboration, *The IceCube high-energy starting event sample: Description and flux characterization with 7.5 years of data*, *Phys. Rev. D* **104** (2021) 022002 [arXiv:2011.03545] [INSPIRE].

[39] IceCube collaboration, *Energy Reconstruction Methods in the IceCube Neutrino Telescope*, 2014 *JINST* **9** P03009 [arXiv:1311.4767] [INSPIRE].

[40] G. D'Amico, *Flavor and energy inference for the high-energy IceCube neutrinos*, *Astropart. Phys.* **101** (2018) 8 [arXiv:1712.04979] [INSPIRE].

[41] IceCube collaboration, *Observation of high-energy neutrinos from the Galactic plane*, *Science* **380** (2023) adc9818 [arXiv:2307.04427] [INSPIRE].

[42] P. Coppin, *GRBweb*, https://icecube.wisc.edu/~grbweb_public, last retrieved on 12 February (2025).

[43] J. Greiner, https://www.mpe.mpg.de/~jcg/grbgen.html, last retrieved on 20 February (2025).

[44] M. Ackermann et al., *The radio/gamma-ray connection in Active Galactic Nuclei in the era of the Fermi Large Area Telescope*, *Astrophys. J.* **741** (2011) 30 [arXiv:1108.0501] [INSPIRE].

[45] V. Vasileiou et al., *Constraints on Lorentz Invariance Violation from Fermi-Large Area Telescope Observations of Gamma-Ray Bursts*, *Phys. Rev. D* **87** (2013) 122001 [arXiv:1305.3463] [INSPIRE].

[46] MAGIC et al. collaborations, *Bounds on Lorentz invariance violation from MAGIC observation of GRB 190114C*, *Phys. Rev. Lett.* **125** (2020) 021301 [arXiv:2001.09728] [INSPIRE].

[47] G. Fiorentini and G. Mezzorani, *Solar neutrinos, sunspot number and the magnetic field in the convective zone*, *Phys. Lett. B* **253** (1991) 181 [INSPIRE].

[48] J. Ludescher et al., *Improved El Niño forecasting by cooperativity detection*, *Proc. Nat. Acad. Sci.* **110** (2013) 11742.

[49] F.W. Stecker, S.T. Scully, S. Liberati and D. Mattingly, *Searching for Traces of Planck-Scale Physics with High Energy Neutrinos*, *Phys. Rev. D* **91** (2015) 045009 [arXiv:1411.5889] [INSPIRE].

[50] D. Colladay and V.A. Kostelecky, *Lorentz violating extension of the standard model*, *Phys. Rev. D* **58** (1998) 116002 [hep-ph/9809521] [INSPIRE].

[51] R. O'Rourke Brogan et al., GCN Circ. 32710 (2022).

[52] P.A.C. Cunha et al., GCN Circ. 32742 (2022).

[53] H. Fausey et al., GCN Circ. 32471 (2022).

[54] D.B. Malesani et al., GCN Circ. 31324 (2021).

[55] M. Ferro et al., *A search for the afterglows, kilonovae, and host galaxies of two short GRBs: GRB 211106A and GRB 211227A*, *Astron. Astrophys.* **678** (2023) A142 [arXiv:2309.03000] [INSPIRE].

[56] A.J. Levan et al., GCN Circ. 31235 (2021).

[57] J.C. Rastinejad et al., *A kilonova following a long-duration gamma-ray burst at 350 Mpc*, *Nature* **612** (2022) 223 [arXiv:2204.10864] [INSPIRE].

[58] D.A. Kann et al., GCN Circ. 29296 (2021).

JCAP02(2026)035

[59] A. Hennessy et al., *A LOFAR prompt search for radio emission accompanying X-ray flares in GRB 210112A*, *Mon. Not. Roy. Astron. Soc.* **526** (2023) 106 [arXiv:2308.16121] [INSPIRE].

[60] L. Izzo et al., GCN Circ. 23488 (2018).

[61] M.H. Siegel and J.K. Cannizzo, GCN Circ. 23499 (2018).

[62] J. Selsing et al., *The X-shooter GRB afterglow legacy sample (XS-GRB)*, *Astron. Astrophys.* **623** (2019) A92 [arXiv:1802.07727] [INSPIRE].

[63] N.R. Tanvir et al., GCN Circ. 18100 (2015).

[64] F. Knust et al., *Long optical plateau in the afterglow of the short GRB 150424A with extended emission — Evidence for energy injection by a magnetar?*, *Astron. Astrophys.* **607** (2017) A84 [arXiv:1707.01329] [INSPIRE].

[65] A. Chrimes et al., *Investigating a population of infrared-bright gamma-ray burst host galaxies*, *Mon. Not. Roy. Astron. Soc.* **478** (2018) 2 [arXiv:1804.08971] [INSPIRE].

[66] J. Elliott et al., GCN Circ. 14898 (2013).

[67] S. Jeong et al., *The dark nature of GRB 130528A and its host galaxy*, *Astron. Astrophys.* **569** (2014) A93 [arXiv:1404.0939] [INSPIRE].

[68] J. Elliott et al., *Prompt emission of GRB 121217A from gamma-rays to the near-infrared*, *Astron. Astrophys.* **562** (2014) A100 [arXiv:1312.4547] [INSPIRE].

[69] S. Schmidl et al., GCN Circ. 13992 (2012).

[70] S.T. Holland, E.A. Helder and D. Xu, GCN Circ. 14003 (2012).

[71] V. Sudilovsky et al., GCN Circ. 13219 (2012).

[72] E. Berger, GCN Circ. 12193 (2011).

[73] S. Piranomonte et al., GCN Circ. 11530 (2011).

[74] S. Campana et al., GCN Circ. 11195 (2010).

[75] S.R. Oates et al., *A correlation between intrinsic brightness and average decay rate of Swift UVOT GRB optical/UV light curves*, *Mon. Not. Roy. Astron. Soc.* **426** (2012) 86 [arXiv:1208.1856] [INSPIRE].

[76] S. Campana and D. Grupe, GCN Circ. 10940 (2010).

[77] S.B. Cenko et al., GCN Circ. 10946 (2010).

[78] A. Nicuesa Guelbenzu et al., *Identifying the host galaxy of the short GRB 100628A*, *Astronomy & Astrophysics* **583** (2015) A88.

[79] T. Krühler et al., *GRB hosts through cosmic time — VLT/X-Shooter emission-line spectroscopy of 96 γ-ray-burst-selected galaxies at* $0.1 < z < 3.6$, *Astron. Astrophys.* **581** (2015) A125 [arXiv:1505.06743] [INSPIRE].

[80] S. Campana, P.A. Evans and S.T. Holland, GCN Circ. 10588 (2010).

[81] J.R. Cummings et al., GCN Circ. 10428 (2010).

[82] S. Dichiara et al., *Short gamma-ray bursts within 200 Mpc*, *Mon. Not. Roy. Astron. Soc.* **492** (2020) 5011 [arXiv:1912.08698] [INSPIRE].

[83] A. Cucchiara et al., GCN Circ. 10422 (2010).

[84] Y. Li et al., GCN Circ. 10913 (2010).

JCAP02(2026)035

[85] D.A. Perley et al., *A Population of Massive, Luminous Galaxies Hosting Heavily Dust-Obscured Gamma-Ray Bursts: Implications for the Use of GRBs as Tracers of Cosmic Star Formation*, *Astrophys. J.* **778** (2013) 128 [arXiv:1301.5903] [INSPIRE].

[86] E. Berger, *A Short GRB 'No-Host" Problem? Investigating Large Progenitor Offsets for Short GRBs with Optical Afterglows*, *Astrophys. J.* **722** (2010) 1946 [arXiv:1007.0003] [INSPIRE].

[87] W.-F. Fong and E. Berger, *The Locations of Short Gamma-ray Bursts as Evidence for Compact Object Binary Progenitors*, *Astrophys. J.* **776** (2013) 18 [arXiv:1307.0819] [INSPIRE].

[88] D.A. Perley et al., GCN Circ. 8914 (2009).

[89] R. Filgas et al., GCN Circ. 7747 (2008).

[90] C. Clemens et al., *GRB 071028B, a burst behind large amounts of dust in an unabsorbed galaxy*, *Astron. Astrophys.* **529** (2011) A110 [arXiv:1103.6130] [INSPIRE].

[91] P. Jakobsson et al., GCN Circ. 6398 (2007).

[92] L. Xiao and B.E. Schaefer, *Estimating Redshifts for Long Gamma-Ray Bursts*, *Astrophys. J.* **707** (2009) 387 [arXiv:0910.4945] [INSPIRE].

[93] N.R. Tanvir et al., *The extreme, red afterglow of GRB 060923A: Distance or dust?*, *Mon. Not. Roy. Astron. Soc.* **388** (2008) 1743 [arXiv:0803.4100] [INSPIRE].

[94] A. de Ugarte Postigo et al., *GRB 060121: Implications of a Short/Intermediate Duration Gamma-Ray Burst at High Redshift*, *Astrophys. J. Lett.* **648** (2006) L83 [astro-ph/0605516] [INSPIRE].

[95] A. Grazian, GCN Circ. 4545 (2006).

[96] E. Berger, GCN Circ. 3962 (2005).

[97] E. Berger, M.-S. Shin, J.S. Mulchaey and T.E. Jeltema, *Galaxy Clusters Associated with Short GRBs. 1. The Fields of GRBs 050709, 050724, 050911 and 051221A*, *Astrophys. J.* **660** (2007) 496 [astro-ph/0608498] [INSPIRE].

[98] J.X. Prochaska et al., *The galaxy hosts and large-scale environments of short-hard gamma-ray bursts*, *Astrophys. J.* **642** (2006) 989 [astro-ph/0510022] [INSPIRE].

[99] P. Ferrero et al., *Constraints on an optical afterglow and on supernova light following the short burst GRB 050813*, *Astron. J.* **134** (2007) 2118 [astro-ph/0610255] [INSPIRE].

[100] P. Schady et al., *Swift-uvot observations of the x-ray flash 050406*, *Astrophys. J.* **643** (2006) 276 [astro-ph/0601182] [INSPIRE].

[101] D.B. Fox, GCN Circ. 2630 (2004).

[102] A.M. Soderberg et al., *An HST search for supernovae accompanying x-ray flashes*, *Astrophys. J.* **627** (2005) 877 [astro-ph/0502553] [INSPIRE].

[103] A. Levan et al., *Infrared and Optical Observations of GRB 030115 and its Extremely Red Host Galaxy: Implications for Dark Bursts*, *Astrophys. J.* **647** (2006) 471 [astro-ph/0608166] [INSPIRE].

[104] A. Gal-Yam et al., *The progenitors of short-hard gamma-ray bursts from an extended sample of events*, *Astrophys. J.* **686** (2008) 408 [astro-ph/0509891] [INSPIRE].

[105] L. Christensen, J. Hjorth and J. Gorosabel, *Photometric redshift of the GRB 981226 host galaxy*, *Astrophys. J. Lett.* **631** (2005) L29 [astro-ph/0508227] [INSPIRE].

JCAP02(2026)035

[106] J.S. Bloom et al., *The unusual afterglow of GRB 980326: Evidence for the gamma-ray burst — supernova connection*, *Nature* **401** (1999) 453 [astro-ph/9905301] [INSPIRE].

[107] M. Stamatikos et al., GCN Circ. 11991 (2011).

[108] De Ugarte Postigo et al., GCN Circ. 11993 (2011).

[109] D'Avanzo et al., GCN Circ. 11997 (2011).

[110] A.Y. Lien et al., GCN Circ. 12774 (2011).

[111] A. Cucchiara et al., GRB Circ. 12777 (2011).

[112] V. N. Yershov et al., GCN Circ. 13796 (2012).

[113] N.R. Tanvir et al., *The Properties of GRB 120923A at a Spectroscopic Redshift of* $z \approx 7.8$, *Astrophys. J.* **865** (2018) 107 [arXiv:1703.09052] [INSPIRE].

[114] https://icecube.wisc.edu/news/research/2014/05/growing-astrophysical-neutrino-signal-in-icecube-now-features-2-pev-neutrino/.

[115] S. Immler et al., GCN Circ. 13727 (2012).

[116] O.E. Hartoog et al., GCN Circ. 13730 (2012).

JCAP02(2026)035